PHILOSOPHICAL TRANSACTIONS OF THE ROYAL SOCIETY A MATHEMATICAL, PHYSICAL & ENGINEERING SCIENCES

The Tides of the Atlantic Ocean, 60 degrees N to 30 degrees S

D. E. Cartwright, R. Spencer, J. M. Vassie and P. L. Woodworth

Phil. Trans. R. Soc. Lond. A 1988 **324**, 513-563
doi: 10.1098/rsta.1988.0037

Phil. Trans. R. Soc. Lond. A **324**, 513–563 (1988) [513]
Printed in Great Britain

THE TIDES OF THE ATLANTIC OCEAN, 60° N TO 30° S

By D. E. CARTWRIGHT, F.R.S., R. SPENCER, J. M. VASSIE and P. L. WOODWORTH

Institute of Oceanographic Sciences†, *Bidston Observatory, Birkenhead L43 7RA, U.K.*

(*Received* 4 *March* 1987)

CONTENTS

As a sequel to Cartwright *et al.* (*Phil. Trans. R. Soc. Lond.* A**298**, 87–139 (1980)) (C.E.S.V.) an extended series of oceanic tidal pressure measurements in the Atlantic Ocean is described and the spatial properties of their spectral components are analysed.

† Now Proudman Oceanographic Laboratory.

 [Published 19 April 1988

The principal linear admittances vary widely across the ocean basins, and clearly indicate the positions of the major amphidromes. Constants for the leading harmonics M_2 and S_2 are defined everywhere along the parallel of 53.6° N and along a section from Natal (Brazil) and west Africa by interpolation between measurements.

From a unique set of seven one-year deep pressure records between 57° N and the Equator, the radiational component of S_2 is shown to have similar magnitude and phase anomaly to values previously known only at coastal stations, confirming its intrinsically atmospheric forcing. From the same records, nonlinear terms in the semidiurnal band are found to be irregular and indistinguishable from noise. From the full set of data, the M_4 overtide is generally small and erratic, probably affected in some areas by low-stability internal waves.

The long-period tides Mm and Mf are clearly identified in the equatorial zone as coherent motions with slight phase variations. Their amplitudes are significantly greater than those deduced from the 'self-consistent equilibrium theory' of Agnew & Farrell (*Geophys. Jl R. astr. Soc.* **55**, 171–181 (1978)).

The M_1 tide, linearly driven from the third-degree harmonic of the potential, has been extracted from multiyear records at 13 representative coastal stations in both hemispheres. It is shown to agree well with a synthesis of normal modes of oscillation computed by Platzman (*J. Phys. Oceanogr.* **14** (10), 1521–1550 (1984)), provided a general phase adjustment of about 60° is made to the synthesized phases. The other third-degree term M_3 is well extracted from most of the pelagic stations but is found to be too finely structured in space for easy interpolation. Attempts are made to model the M_3 tide from sums of normal modes and from Proudman functions (defined in §5*a*) with only moderate success, owing to noisy coastal data.

High solar harmonics from the atmospheric tide penetrate to the ocean bottom, and are especially noticeable at low latitudes. The ter-diurnal solar pressure close to S_3 is shown to have similar spectral characteristics in midocean to that calculated from the fourth harmonic of the radiational potential of Munk & Cartwright (*Phil. Trans. R. Soc. Lond.* A**259**, 533–581 (1966)). At coastal stations, however, the S_3 line itself dominates, probably because of the thermal responses of the conventional tide gauge and of shallow coastal waters.

Representative diurnal and semidiurnal harmonics are mapped spatially by the 'objective analysis' procedure of Sanchez *et al.* (*Mar. Geod.* **9** (1), 71–91 (1985)), with a set of basis (Proudman) functions computed for the Atlantic-plus-Indian Oceans by D. B. Rao. Data from both oceans are used in the fits but the results are probably most accurate in the Atlantic Ocean on account of the greater concentration of pelagic data. The first 100 Proudman functions out of 470 computed by Rao are found to fit the M_2 data (50 for O_1) optimally, without 'over-fitting'. Goodness of fit is biased towards areas of greater amplitude. Most of the known features of tidal maps are reproduced fairly well, but the anti-amphidrome of M_2 in the Indian Ocean has too large amplitude. Inaccuracy is attributed to the dearth of pelagic tidal data in the Indian Ocean.

The same constituents are similarly mapped by empirically fitting sums of Platzman's normal mode functions to the same data. Numbers of basis functions here should, in principle, be restricted by the need for reasonably small values of (natural frequency of mode minus tidal frequency). About 20 Platzman modes give a reasonable mapping of O_1, less successfully for M_2, but the fits are generally less good than those from 50–100 Proudman functions.

A calculation of the work done by the Moon on the Atlantic tidal field defined by the Proudman-function synthesis confirms that this parameter is the net sum of nearly cancelling positive and negative zones, and is therefore sensitive to small errors in the tidal field.

In summary, there remains a mismatch between the precision and detail of tidal parameters known at a finite number of measuring points and spatial interpolations derived from present computational schemes.

PHILOSOPHICAL TRANSACTIONS OF THE ROYAL SOCIETY A MATHEMATICAL, PHYSICAL & ENGINEERING SCIENCES

1. Introduction

This paper is a sequel to Cartwright, Edden, Spencer & Vassie (1980) (henceforth C.E.S.V.), which concentrated on the tides of a small portion of the North Atlantic between the Mid-Atlantic Ridge and the west European shelf. In both works we have aimed to discover what can be learnt of the spatial dynamic properties of the ocean tides from direct measurements in the open sea, with a minimum of prejudice from the artefacts of computer models. An essential background has been a development over roughly 15 years (1970–1985) of the instrumental technique of recording pressure variations on the ocean floor for long periods, together with their associated acoustic recall systems and calibrating devices. This instrumental development has been led principally by one of the authors (R.S.) with the help of colleagues at the Bidston and Wormley laboratories of the Institute of Oceanographic Sciences (IOS).

The sea-going activity described in C.E.S.V. had seemed adventurous, because tidal variations offshore had not been measured before in that part of the Atlantic Ocean, but when compared with computer-generated tidal maps of the world ocean the distances reached appear small on the scale of the principal wavelengths. Similar measurements in the Atlantic by other authorities were concentrated in a narrow band within a few hundred kilometres of the east coasts of Canada and the U.S.A. (Cartwright *et al.* 1979). With the sanction of the IOS we decided to bridge the gap between east and west Atlantic by a few supplementary lines of pressure recordings between the existing sets. Some pressure records from the equatorial zone taken later as part of a climate research programme (Cartwright *et al.* 1987) extended the network further to the south. We shall be concerned here with the analysis of these new data sets and with the interpretation of the whole available set of tidal constants from the Atlantic Ocean including islands and coasts.

After describing our second campaign of measurements and how we processed the results, we shall outline some semiquantitative facts arising from them concerning spatial variation in linear admittance functions, the positions of major amphidromes in the North and South Atlantic, and the distribution of amplitude and phase of the semidiurnal tides across open boundaries between the continents. This section is concluded with evaluations of anomalous semidiurnal effects such as the radiational content of S_2 and triple interaction terms such as $2MS_2$, and a brief discussion of the distribution of the overtide M_4.

In the following section, we discuss some more subtle tidal components, most of which are extractable only from long periods of data. These include the long period tides Mm and Mf and some components that arise linearly from the third-degree harmonic in the gravitational potential, namely M_1 and M_3. We also show that high solar harmonics from the atmospheric tide are prominent in ocean-pressure records at low latitudes and discuss the component which is centred on S_3, itself basically due to the fourth harmonic of the radiational potential.

Finally, we return to the fundamental problem of mapping the principal diurnal and semidiurnal tides from the new set of data, including coastal values. We investigate forms of expansion of the oceanic tidal field in series of basis functions, in particular the set of normal modes of the world ocean computed by G. W. Platzman and his colleagues, and the more primitive 'Proudman functions' computed for the Atlantic and Indian Ocean basins by D. B. Rao and his colleagues. To do this we had to use coastal data from the Indian as well as the Atlantic Ocean, but attention is focused on the mapping of the Atlantic Ocean where it is clearly more accurate.

Some sets of harmonic constants which are not available from presently published compilations are tabulated in Appendixes A and B.

2. Data acquisition

(*a*) *Instrumental technique*

The tidal elevation relative to the sea bed is measured in the open sea by recording the variations in pressure at an instrument resting on the sea bed. After a suitable period of recording the instrument is recalled to the surface by acoustic signals from the parent ship. The principles of the specialized techniques involved have been known for over 20 years with their successive improvements. In C.E.S.V. we outlined the development of our instrumental technique at IOS (and previously at the National Institute of Oceanography at Wormley), from capacitance-plate pressure sensors operating down to 200 m depth to strain-gauge sensors operating down to about 3800 m. Recording duration improved from one to three months with the introduction of lightweight cassette recorders, leading to the IOS 'Mark 4' design of pressure recording assembly.

Since 1978 we have continued to improve the 'Mark 4' assembly, chiefly by the introduction of the 'digiquartz' crystal sensor of American manufacture, with its extremely low temperature sensitivity, creep rates less than 50 mbar† in three months, and depth range more than 5500 m. Duration capability has also been improved to more than 14 months, with 6 channels recorded at a rate of 4 h^{-1}. In short, all aspects of recording techniques have been improved in the years following the work reported in C.E.S.V. Consequently, as well as having much cleaner records we are no longer restricted by depth limitations or the need to recover instruments after a month or two as previously. Each instrument assembly invariably includes two independent pressure transducers with associated temperature sensors, thereby providing useful redundancy. Only two units have been irretrievably lost due to release or buoyancy failure in over 50 deep moorings.

Further details of instrumental performance and calibration are described by Spencer & Vassie (1985), including the effective elimination of creep in the digital pressure series by means of an empirically fitted monotonic function with four independent parameters. For an alternative and equally well studied approach to deep-sea pressure recording technique see Filloux (1980).

(*b*) *Ship campaigns and strategy*

Our attempts to bridge the gaps between existing data stations in the eastern and western zones and between the continental coasts were governed largely by the availability of research vessels in suitable areas. An additional constraint was the need to visit each station twice, once to lay instruments then to recover them after 1–12 months. The principal lines of stations covered, with dates, were between

(i) Guinea-Bissau (West Africa) and Natal (North Brazil), 1978;
(ii) Azores islands and St John's (Newfoundland), 1980–1;
(iii) Azores islands and Iles du Salut (French Guiana), 1981–2.

† 1 bar = 10^5 Pa.

The cruise-tracks of the R.V. *Discovery* associated with (i) enabled us to place an additional recorder in the tidally controversial area west of Saint Helena (Cartwright 1971), to be recovered later in 1979 from the French V.O. *Jean Charcot* by courtesy of CNEXO. Co-operation with the Brazilian Directorate of Hydrography and Navigation and with the Instituto Oceanografico of São Paulo resulted in access to new data of good quality from Brazilian islands and ports and some pelagic records along the shelf edge.

For the line (ii) we co-operated with the Canadian Hydrographic service (CHS) who provided some shallow stations from the Grand Banks area and a deep station from the region of 'Milne Seamount'† where our nearby recorder malfunctioned. The CHS also took a tidal record from the shelf edge west of Cartwright, Laborador, which is in the same latitude, 53° 36′ N, as our earlier line of stations between Inishbofin and the Ridge at 20° W. Financial restrictions caused us to abandon plans to complete the Inishbofin–Cartwright line, which would have provided a northern boundary for Atlantic models, complementary to line (i), but we shall make some plausible interpolations in §3.

In addition to the above strategy we have also used 'ships of opportunity' to lay and recover seven long-term moorings each of approximate duration one year at a range of latitudes from 57° N to the Equator. Their code letters, locations and times are listed in table 1. Station Y1 was actually a sequence of two consecutive recording periods at two sites 10 miles apart with combined duration 11 months. YN and YP used the 'Teleost' system of pressure recording, devised by Mr A. J. Harrison of IOS, whereby the frequency of a 'digiquartz' crystal is integrated for 15 min and logged by the 'Aanderaa' mechanism. All other stations in table 1 were recorded by the 'Mark 4' system described above. Stations FP1-FP3-FP4 were an IOS appendix to the French 'FOCAL' exercise in monitoring the thermodynamic processes along the Atlantic Equator. Although the object of these last three stations was primarily for the study of subtidal frequencies (Cartwright *et al.* 1987) they also provided a useful addition to the present series of long-term tidal information.

TABLE 1. LONG-TERM PELAGIC TIDAL STATIONS

station code	latitude / deg N	longitude / deg W	depth/m[a]	date span (year/month)
YN	57	10	2120	1981/7–1982/7
YP	51	13	2085	1983/5–1984/5
Y1	45	16	3000	1980/7–1981/7
Y2	34	29	3294	1982/3–1983/3
FP1	0	20	2750	1983/2–1984/2
FP3	0	10	4100	1983/2–1984/2
FP4	0	−6	3065	1983/5–1984/5

[a] Approximate depths, based on a nominal acoustic speed of 1.5 km s^{-1}.

Finally a few additional tidal stations in areas relevant to the deep ocean have arisen from instrument tests and other field exercises not directly involving tidal research.

The positions of all existing tidal stations in the open Atlantic Ocean north of 30° S are marked in figure 1, where distinctions are made between stations taken by IOS, stations taken by other authorities, principally North American, and island stations which are effectively pelagic as far as tides are concerned. No attempt has been made to show the many very shallow

† This is erroneously marked on some charts as a shallow bank.

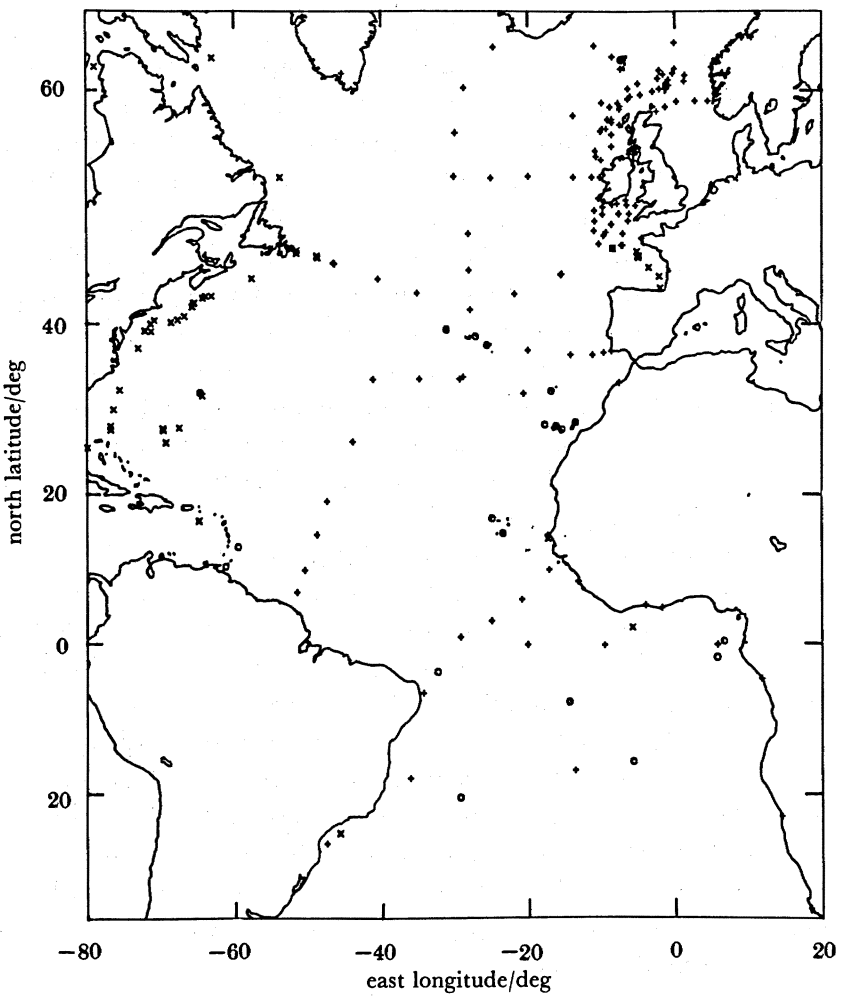

FIGURE 1. Map of all important pelagic and island tidal data in the Atlantic Ocean. +, Pelagic data from IOS; ×, pelagic data by other organizations; ○, reliable island data, excepting Tristan da Cunha (37° S, 13° W), which is off the map.

water stations that exist, especially in the British and Canadian shelf areas, or the numerous mainland tide gauges whose tidal constants are well known from the compilations of the International Hydrographic Bureau (IHB), Monaco.

Within the area of figure 1 there are altogether 153 pelagic tidal stations, of which 96 are from the IOS programme. The geographical coordinates and leading harmonic constants of all these stations with other relevant details are listed in §§ 1.1, 1.2, 1.3 and 1.4 of the compilations of Cartwright *et al.* (1979) and Cartwright & Zetler (1985).

(*c*) *Island and mainland stations*

As we pointed out in C.E.S.V. accurate data from small remote islands are more important to oceanic tide research than to the conventional needs of navigation. Accordingly, as before, we have collected new and greatly improved data from most of the Atlantic islands (excluding the Caribbean islands which are outside our area of study) during this programme. Mention has already been made of help from Brazilian authorities which furnished one-year data sets from Trindade and Fernando de Noronha islands and some new data from the Brazilian

mainland. Tidal constants for St Peter and Paul Rocks (1° N, 29° W) were derived for the first time from one of the IOS pelagic records as part of exercise (i) above. Other pressure records from this locality have since been taken by the French ORSTOM group.

We point out particularly that the early set of tidal constants for Isla da Trindade, published in table 3 of Cartwright (1971), have been completely superseded by our more recent evaluation (Appendix A) and also by some official Brazilian lists. The 1961 data set was short in duration, poorly recorded and specified in the wrong time zone. The correct phase lags of the tidal harmonics at Trindade listed here result from a year of properly recorded data in 1974 and are closer to the corresponding phase lags on the Brazilian mainland at the same latitude, as one would expect from the computed tidal maps of Schwiderski (1983), for example.

Monsieur J.-M. Verstraete of the French Office de Recherche Scientifique et Technique d'Outre Mer (ORSTOM) kindly supplied us with a year of data from the islands of São Tomé and Annobon and the mainland port of Pointe Noire (Congo) taken during the FOCAL exercise, 1983–1984. The ORSTOM station at São Tomé is at the extreme southern tip of the main island, very close to the Equator; tidal constants for Annobon (2° S, 6° E) were previously unknown. The Portuguese Instituto Hidrografico supplied us with recent 1 year analyses from tide gauges at Madeira and Flores (39½° N, 31° W). Our own recordings associated with the 'World Ocean Circulation Experiment' have furnished improved tidal constants for the British islands of Ascension, Saint Helena and Tristan da Cunha (37° S, 12½° W).

Harmonic constants from the islands mentioned above and a few other islands not included in C.E.S.V. are listed in Appendix A, to which we have added some mainland stations whose constants are either missing from the IHB compilations or are considered by us to be more accurate than those compilations and those listed in the *Admiralty tide tables*.

(*d*) *Methods of data analysis*

In C.E.S.V. we had to deal with rather short pelagic records from 10–40 days long for which the conventional methods of spectral analysis were inaccurate and ill-suited. We adopted instead a scheme described in Cartwright *et al.* (1969) whereby all pelagic records are correlated with a synthetic tidal series computed for the same period from a full set of 'response' weights appropriate to certain 'reference stations'. Eight reference stations were chosen from coastal tide gauges around the area of study, the response weights from each having been carefully defined from 6–9 years of data. The corresponding admittance functions of these stations were shown to be closely interrelated.

Among the present records, only those taken during exercise (i) were analysed by the above procedure, being only 29 days long. For these we at first used Ascension Island as a 'reference station', as in Cartwright (1971), but its diurnal admittance was later deemed to be untypical of the northern tropics so it was replaced, several years later, by our 1 year pressure station FP1 (table 1). A few other short pressure records taken primarily for instrument tests were also analysed with respect to nearby coastal stations possessing at least 1 year of good tidal data.

After exercise (i), most of our records were more than three months long, so we found it more satisfactory to extract their tidal constants by the original method of Munk & Cartwright (1966), with respect to computed time series for the gravitational and radiational potentials. This clearly makes a more unified approach, especially because suitable reference stations

become very sparse towards the tropical Atlantic, and their admittance functions change shape dramatically (see §3).

It may be queried whether one may adequately resolve the radiational and gravitational responses at the solar frequencies, especially around S_2, from data of only 3 months. Certainly, one cannot use the lunar modulation at the sidereal frequencies K_1 and K_2, as for example in Munk & Cartwright (1966) (see also Cartwright & Edden 1977), because this requires an order of 18 years. However, the radiational component at S_2 is so much larger than at K_2 that any analysis which can resolve these two distinct tidal constituents can give a fair representation of the radiational contribution to the solar tide. Six months are clearly just sufficient for this, and in fact three months are adequate at the low noise levels of oceanic pressure. The diurnal radiational tide, principally at S_1, is very small in the Atlantic Ocean and was neglected in most of our analyses.

When it came to the 1 year pressure records, there was interest in resolving not only the radiational tides but also the triple interactions (for example $2MS_2$) within the semidiurnal band, basically due to nonlinear frictional stresses. There is a procedure for accommodating such terms in a 'response' analysis (see, for example, Munk & Cartwright 1966), but it is not entirely satisfactory for various reasons. For simplicity we evaluated these terms directly from the conventional harmonic constants from a year's data. Specifically, we fit three-parameter splines in frequency through the quasi-admittances

$$Z(f) = H/H_p \exp(-iG)$$

derived from three harmonic pairs (H, G) known to be dominantly linear related to the gravitational potential amplitude H_p. Splines took the form

$$Z(f) = a\cos 2\pi k(f-f_M) + b\sin 2\pi k(f-f_M) + c, \tag{1}$$

where f_M is the frequency of M_2, $k = 2d$, and a, b, c were complex coefficients adjusted to fit the constituents N_2, M_2, K_2 (for examination of anomalies at L_2, S_2), or $2N_2$, N_2, M_2 (for examination of the nonlinear anomaly at μ_2). The anomaly itself was extracted from a 'constituent' (H', G') at frequency f' as

$$A(f') = H' \exp(-iG') - H'_p Z(f'), \tag{2}$$

where H'_p is the linear potential amplitude at that frequency. When applied to the radiational anomaly at S_2 the above method is similar to one used by Zetler (1971).

All sets of the leading linear harmonic tidal constituents

$$Q_1, O_1, P_1, K_1; N_2, M_2, S_2, K_2; \text{ in some cases } M_3,$$

derived from our pelagic pressure records and all other such pelagic records from international sources have been compiled in the IAPSO *Publications Scientifiques* nos 30 and 33 (Cartwright *et al.* 1979; Cartwright & Zetler 1985). The compilations include direct evaluations of noise and signal variances from which one may estimate standard errors. These vary with the duration of the analysed record, the level of oceanic noise and quality of the pressure sensor, so it is difficult to make broad generalizations.

Table 2 lists the relative standard errors (RSE) of harmonic amplitudes and phases in the diurnal and semidiurnal bands at four contrasting stations, computed from an approximate formula quoted in C.E.S.V., equation (5). (For a more detailed discussion of the variance of

TABLE 2. STANDARD ERRORS AT TYPICAL PELAGIC STATIONS

station code	latitude deg N	longitude deg W	depth/m	duration/d	diurnal RSE	diurnal phase	semidiurnal RSE	semidiurnal phase
T4	1	29	352	29	6.6	3.8°	1.0	0.6°
A1	46	47	525	118	2.9	1.7°	0.7	0.4°
G2	19	48	3470	90	4.0	2.3°	0.8	0.4°
FP1	0	20	2750	412	1.2	0.7°	0.1	0.1°

tidal harmonics see Cartwright & Amin (1986).) Station T4 was on the St Peter and Paul Rocks seamount, recorded for only 29 days by a 'Mark 3' assembly with strain gauge sensor. Station A1 was on Beothuk Knoll near the shelf break of the Newfoundland Grand Banks, a location with low amplitude tides and considerable weather perturbations, also recorded by a 'Mark 3' assembly but for a longer period than T4. Station G2 was on the mid-Atlantic Ridge at 19° N, a deep location recorded by a 'Mark 4' assembly with 'digiquartz' sensor. Station FP1 was an equatorial station similar to G2 but with over a year's recording.

In general, standard errors are comparable in magnitude at all stations, except for FP1 which also has the best instrumentation as well as a much longer duration. Diurnal relative errors are typically about five times greater than semidiurnal errors because of weak diurnal tidal signals in the Atlantic accompanied by a higher noise continuum at the lower frequency.

3. GENERAL TIDAL CHARACTERISTICS

(a) *Linear admittances*

We conventionally define the 'admittance' at a given place as the complex ratio of the observed tide there to the 'equilibrium tide' at the Greenwich Meridian, as a function of frequency. (The 'latitude factor' is removed from the equilibrium tide; see Munk & Cartwright (1966), Cartwright & Tayler (1971) for the assumed normalization.) The admittance for tidal species m is thus represented as a function of frequency f,

$$Z_m(f) = R_m(f) \exp[-\mathrm{i}G_m(f)], \tag{3}$$

where R_m is the real ratio of the tidal amplitude to the corresponding coefficient in the harmonic expansion of the gravitational tide potential (Cartwright & Taylor 1971), and G_m is the usual Greenwich phase lag. Some authors (for example, McMurtree & Webb 1975), use $+\mathrm{i}G$ in (3); we adopt the minus sign merely for consistency with our earlier work. Munk & Cartwright (1966) discuss methods of evaluation of $Z_m(f)$ without direct recourse to a harmonic expansion. Plots of $Z_m(f)$ add a relevant third dimension to the conventional tidal map at a single harmonic frequency.

In C.E.S.V., we showed diagrams of admittance functions for tidal species $m = 1, 2$ at seven representative coastal locations surrounding the ocean area surveyed in that paper. Admittances for $m = 1$ were of different shape from those for $m = 2$, but the functional shapes for the same species were seen to be closely similar. Only the diurnal admittance at Reykjavik (Iceland) showed signs of a definite spatial change in shape. These similarities were due to the fact that, except for short wavelength topographic diurnal waves, the longer wavelength features of both species of tide in the northeast Atlantic are essentially dominated by simple Kelvin-wavelike propagation.

PHILOSOPHICAL TRANSACTIONS OF THE ROYAL SOCIETY A MATHEMATICAL, PHYSICAL & ENGINEERING SCIENCES

Marked differences in admittance characteristics, such as 'tidal age' around the world oceans are well known (Garrett & Munk 1971; Webb 1973). Our present measurements enable us for the first time to trace such changes continuously across an ocean. Figure 2 shows three representative lines across our area linking mainland coastal sites where tidal constants are well defined through sequences of evenly spaced pelagic stations. Whether the lines are

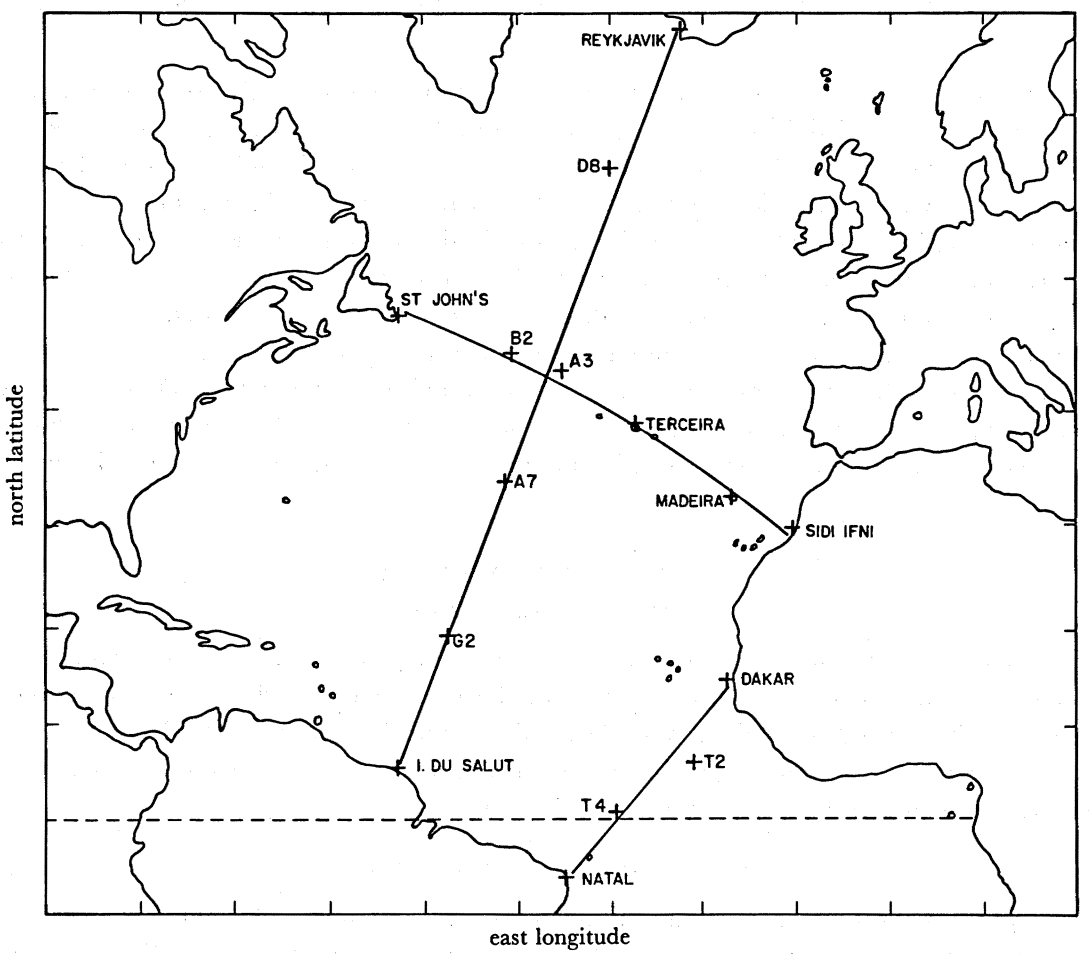

FIGURE 2. Four lines of stations selected for discussion of spatial variation of admittance functions. Crosses show the exact positions of stations (see tables A1 and B1), with pairs of symbols for pelagic stations and names for coastal and island stations.

straight or slightly curved on the given (Mercator) map projection has no significance. Diurnal and semidiurnal admittance functions at all marked stations along these lines are depicted in figure 3*a*, *b*. The quantities plotted are actually the real and imaginary parts of

$$\ln [Z_m(f)] = \ln [R_m(f)] - iG_m(f) \tag{4}$$

for $0.85 < f < 1.05$ d^{-1} (diurnal species) and $1.85 < f < 2.05$ d^{-1} (semidiurnal).

Figure 3*a* shows the variation across the longest section, from Reykjavik to Iles du Salut off French Guiana. The semidiurnal admittances (right) show rather little change in general shape, if we disregard different levels of general amplitude ratio $R(f)$ and phase lag $G(f)$. Only the curves for station A3, which is the closest to the main amphidromic region (see §3*b*), show

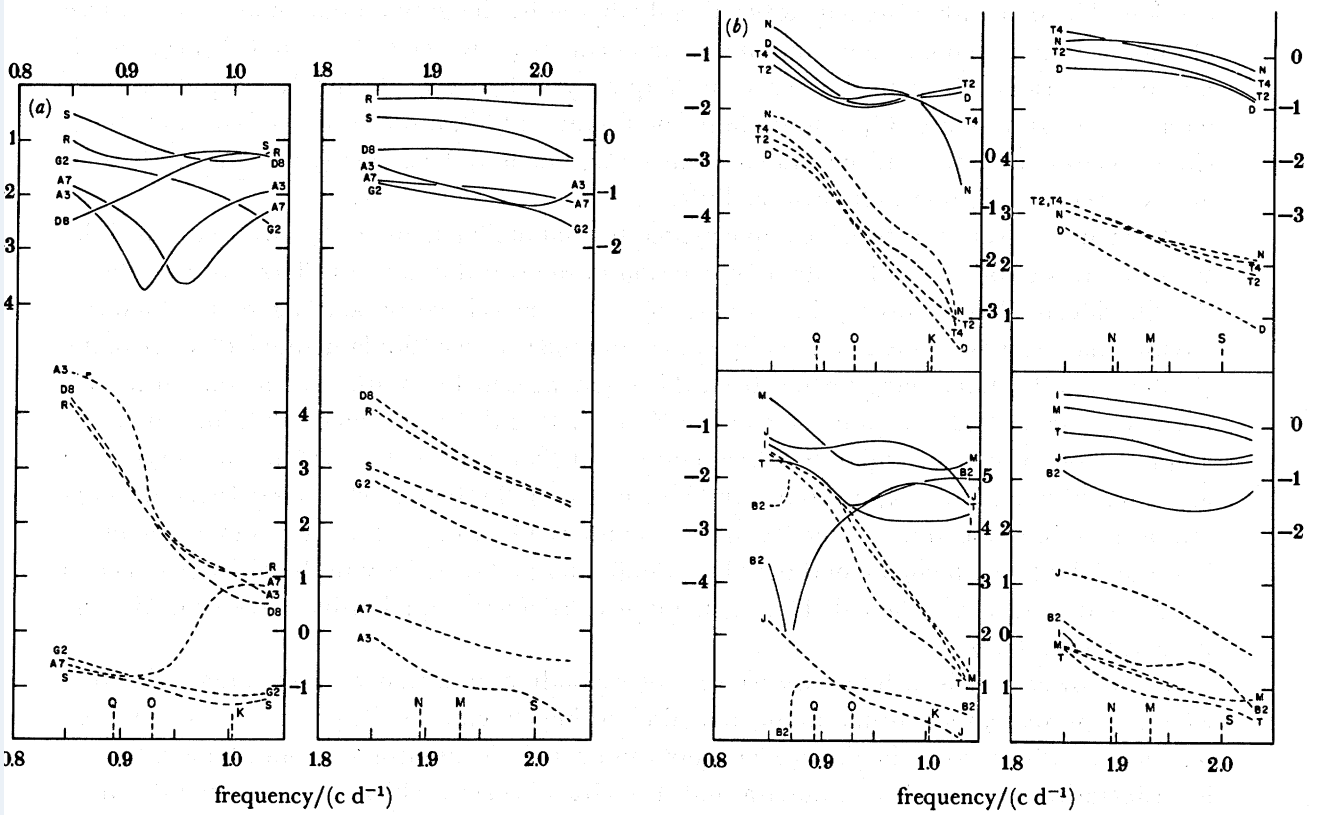

FIGURE 3. (*a*) Real (——) and imaginary (– – – –) parts of ln (*Z*) across the diurnal (left) and semidiurnal (right) tidal bands at the sequence of stations between Reykjavik (R) and Isles du Salut (S) from figure 2. Letters near the base denote the leading harmonic constituents at their appropriate frequencies. (*b*) As (*a*) for lines Natal (N) – Dakar (D) (upper panels) and Sidi Ifni (I) – St John's (J) (lower panels). Other letters denote Madeira (M) and Terceira (T).

a minimum amplitude ratio and some irregularity in phase near the frequency of S_2. As usual, the coastal stations have the largest amplitude ratio owing to the Kelvin-wave effect. Much more drastic changes are seen in the diurnal curves (left). The amplitude ratios clearly pass through a pronounced minimum of increasing frequency from stations A3 to A7, and the phase gradients flip suddenly from steep values north of A3 to gentle gradients south of A7. (The actual position of the O_1 amphidrome, obviously close to A3, will be discussed in the following section.)

It has long been known that the 'age' of the diurnal tides in the Atlantic Ocean, related to their phase-gradients, varies greatly from the northeastern coasts where it is typically five days to the northwestern coasts such as the U.S.A. Atlantic sea board where the age is less than 12 h, but this phenomenon has received little attention because the diurnal amplitudes are relatively low. However, two relevant theoretical studies have appeared in recent years. Huthnance (1983) used a model of greatly simplified geometry, similar to but differing significantly from one proposed by Gill (1979) for the semidiurnal tides, to show the salient features of the diurnal tides in the Atlantic. He showed that the diurnal tides are largely governed by a single-wavelength resonance around the circumpolar Southern Ocean. This gives rise to 'free' waves propagating in the North Atlantic which nearly cancel over a

PHILOSOPHICAL TRANSACTIONS OF THE ROYAL SOCIETY A MATHEMATICAL, PHYSICAL & ENGINEERING SCIENCES

considerable area with a 'forced' wave directly driven by the gravitational potential. Because of this near-cancellation, the amplitudes are generally low and the detailed structure is unusually sensitive to small differences in frequency as between O_1 and K_1. Significant differences are (i) a greater O_1 amplitude in the Southern Ocean owing to its frequency being closer to resonance, and (ii) the tendency for the O_1 tide to radiate energy into the Norwegian Sea whereas the K_1 tide radiates very little.

Huthnance's (1983) picture is complemented by that of Platzman (1984), who expressed the tides in terms of the normal modes of oscillation in the world ocean. In Platzman's synthesis, the O_1 tide is almost entirely in a mode of 28.7 h period, corresponding to Huthnance's circumpolar resonance but described by Platzman (1984) as the 'fundamental half-wave of the Pacific'. The K_1 tide, being further from this resonance, includes also a contribution from a normal mode at 21.2 h, a 'full wave of the Pacific'. It is the 21.2 h mode that introduces an amphidrome in the Norwegian Sea (see figure 17 of Platzman *et al.* 1981) accounting for the low external radiation of K_1 noted by Huthnance (1983). But both modes being driven through spatial-temporal resonances in the Pacific and Southern Oceans, produce only minor 'spillover' into the Atlantic with correspondingly low amplitudes and sensitivity to the differences across the diurnal band already noted. These general properties are in qualitative agreement with the present figure 3*a*, *b*.

In the lower panels of figure 3*b* we see corresponding admittance curves along a section which is approximately normal to the first, also passing close to A3. To provide a roughly even spacing of stations along the line we have not duplicated the admittance from A3 here, but we have included the islands of Madeira and Terceira (Azores), which are conveniently sited. Again, the semidiurnal admittances are roughly similar in shape, with some irregularity at B2 owing to its proximity to the amphidrome, whereas the diurnal admittances are as confused as on the Iceland–Guiana section. At B2 there is apparently an amphidrome at the low frequency edge of the diurnal band, near the small constituent known as $2Q_1$, and Terceira and Madeira show less pronounced minima in $R(f)$. The steep phase gradient evidently holds everywhere east as well as north of A3, and only St John's shows the characteristic low gradient (small age) of the North American coast. The transition from steep to gentle phase gradient is evidently quite rapid, and associated with the amphidromic region where the two sections cross. We should add that Bermuda and all the pelagic stations bordering the U.S.A. coast have slight, that is 'normal' diurnal phase gradients (age).

Finally, the upper panels of figure 3*b* show the results from four representative stations near a short section between Natal and Dakar. A slightly more southerly line lying closer to the pelagic stations T1–T4 is considered in the following section, but it ends in Guinea-Bissau where there is no suitable coastal station for tidal comparison. There is little change in the shape of the semidiurnal admittance curves, and less change across the diurnal band than in the other sections. The pivotal point in amplitude just below 1 d^{-1} seems to be real; the constituent amplitudes for K_1 and J_1 at Dakar are considerably greater than the corresponding values at Natal, whereas Q_1 and O_1 are greater at Natal. It is interesting to see once again the steep diurnal phase gradient across the whole section. 'Normal' phase gradients seem to be confined to relatively narrow zone to the northwest of the basin. As Huthnance (1983) pointed out, there are near-cancellation situations in the South Atlantic as well as in the North. The area of small gradient is probably identifiable with local dominance of the directly forced diurnal wave.

PHILOSOPHICAL TRANSACTIONS OF THE ROYAL SOCIETY A MATHEMATICAL, PHYSICAL & ENGINEERING SCIENCES

(*b*) *Amphidromes and boundary values*

There is a traditional interest in the positions of the major amphidromes north and south of the Equator. The measurement area studied in C.E.S.V. was well to the east of all North Atlantic amphidromes, but we were able to suggest the following tentative positions by extrapolation: M_2 (50° N, 39° W), S_2 (50° N, 36° W), O_1 (40° N, 37° W), K_1 (32° N, 35° W). Our projected northern line at 53.6° N would have fixed the M_2 and S_2 amphidromes with some precision, but we may still improve on the C.E.S.V. estimates by making use of our pelagic stations to the south and west. The diurnal amphidromes are in any case further among the A and G series of stations.

The upper part of figure 4*a* shows the positions of stations some of which we used to re-estimate the North Atlantic amphidromes. The usual method is to interpolate the real and

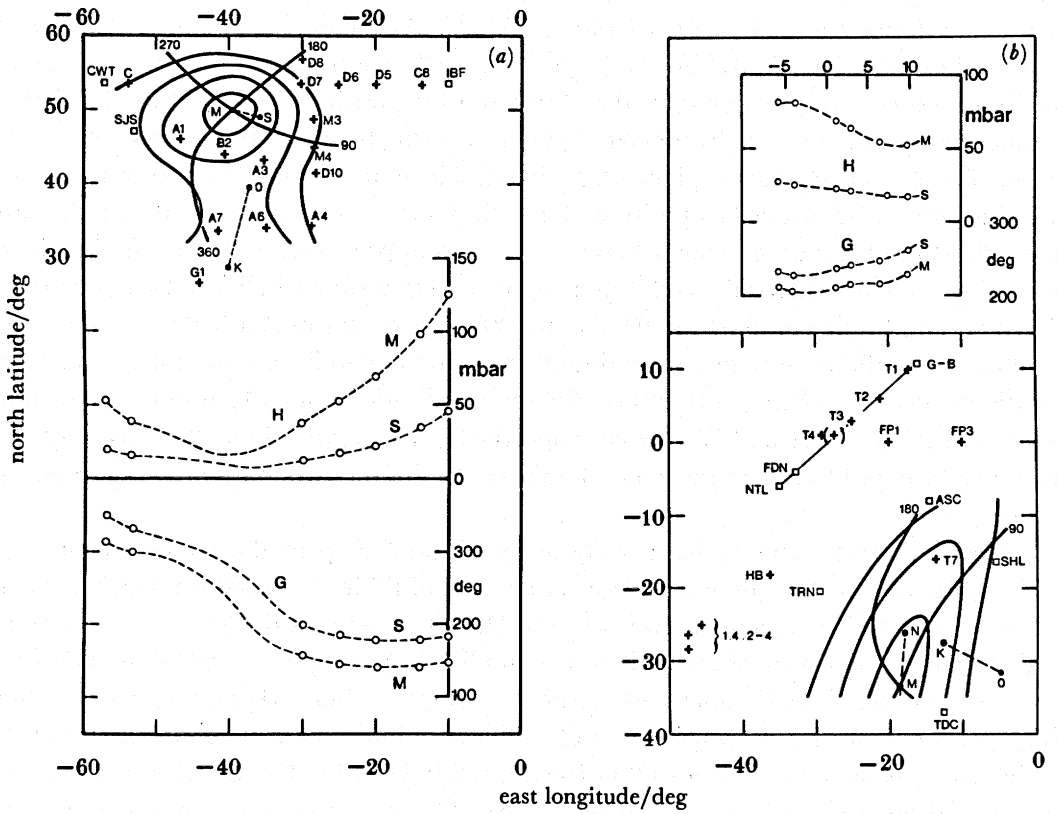

FIGURE 4. (*a*) Top diagram: contours of equal amplitude in steps of 10 mbar outwards from the M_2 amphidrome centre at M, and equal phases 90°, 180°, 270°, 360°, interpolated from some of the stations in the north Atlantic, marked by crosses. Double-lettered symbols (e.g. A3) denote pelagic station-codes. Triple letters denote the coastal stations Cartwright (CWT), St John's (SJS), and Inishbofin (IBF). C denotes a Canadian pelagic station on the Labrador shelf. S, O, K denote the interpolated amphidrome centres of constituents S_2, O_1, K_1, respectively. Lower diagrams: amplitude (H) and phase (G) of M_2 and S_2 along the line CWT–IBF; the circles are measured values, the dashed lines are interpolations. (*b*) Lower diagram: contours of equal M_2 amplitude and phase similar to (*a*) but for southern latitudes. Triple letters denote the pelagic stations FP1, FP3 and the coastal stations Trindade (TRN), Ascension (ASC), St Helena (SHL), Tristan da Cunha (TDC), Natal (NTL), Fernando de Noronha (FDN) and the coast of Guinea-Bissau (G-B). Crosses on extreme left denote three stations on the Brazilian shelf with their serial numbers. The cross in brackets is an adjusted position related to T4 by interpolation. Upper diagram: similar to (*a*) for amplitude and phase of M_2 and S_2 along the line NTL–T1. The top scale indicates the north latitude which corresponds to horizontal position along the line of stations.

imaginary parts of $H \exp(iG)$ to a point where both parts are zero. With three stations around the expected node, one may only interpolate linearly, fixing a set of straight cophase lines and a set of concentric ellipses for the co-amplitude lines. (See Cartwright (1971), where some alternative methods are tried, but without noticeable improvement.) In the present case, for M_2 and S_2 it seems reasonable to use as wide a spread of nearby stations as possible, with a quadratic interpolation scheme.

The cotidal map for M_2 sketched in figure 4*a* was derived from six-parameter quadratic interpolation between stations A1, A3, M3, D7 together with the Canadian stations C and B2, for the area above 45° N. Below 45° N we used A1, B2, A3 as above with A6, A7, G1. The deduced amphidrome is at 50° N, 39.5° W, very close to the position extrapolated (linearly) in C.E.S.V. The corresponding node for S_2 (contours not shown) is also indicated at 49° N, 36° W, only 1° south of our previous estimated position.

Because of the greater uncertainty surrounding the diurnal constants, we used only linear interpolation to derive the nodes of O_1 (triangle B2–A3–A7) and K_1 (triangle A7–A6–G1). The resulting positions (40° N, 37° W) and (28° N, 40° W) are shown in the figure. Both are different from and certainly better than the very tentative positions suggested in C.E.S.V.

The computed tidal maps of Schwiderski (1981, 1983) which are generally considered to be accurate in this part of the ocean, place all their amphidromes within 1° or so of the above 'measured' positions. Schwiderski's position of 49° N, 37.5° W is perhaps a little too far east, but the others give pleasing agreement between the two approaches. There is another small discrepancy between Schwiderski's (1983) map for M_2 and that shown in figure 4*a*. Schwiderski gives closed co-amplitude contours for 10, 20 and 30 cm, whereas ours are closed only for 10 and 20 mbar. The difference between centimetre and millibar units is negligible. In fact our interpretation is nearer to being correct because the amplitudes H for M_2 at our very reliable stations A6 and A7 are 27.1 and 25.9 mbar respectively, not greater than 30 cm as suggested by Schwiderski's map. Otherwise the general appearances of the two maps are very similar in this region.

Having derived what seems to be a fairly accurate tidal map in the region shown, it is reasonable to use their values along the 53.6° N parallel to fill in the positions which we were unable to occupy with instruments between C and D7. The curves in the lower panel of figure 4*a* thus give a complete picture of the variation of amplitude H and phase lag G along the entire line between Cartwright (Labrador) and Inishbofin (Eire) for both M_2 and S_2. Circles show the actual measured values; elsewhere the broken lines are interpolated from other stations as above. The strong Kelvin wave form west of Ireland (cf. figure 10 of C.E.S.V.) is evidently not matched by a similar process in the Labrador Sea. The dynamic situation is confused by secondary amphidromes near Nova Scotia and Baffin Island.

The diurnal tides in the area are too disturbed by topographic wave forms to enable a similar interpolation to be made reliably for O_1 and K_1.

The very existence of semidiurnal amphidromes in the sub-tropical South Atlantic is controversial. One appears as a prominent negatively rotating (i.e. 'con solem') feature in all computed models of the semidiurnal tides which are not constrained to fit the coastal data. Similar features appear in the normal modes of the world ocean of natural period 12.1, 12.5 and 12.8 h which contribute most strongly to the M_2 tide (Platzman *et al.* 1981; Platzman 1984). However, no amphidrome in this area appears in the M_2 model of Parke & Hendershott (1980) or in some less advanced earlier models which are strongly constrained to fit coastal

data. As pointed out by Platzman (1984), this is because the observed phase lags progress northwards on both the African and South American coasts. The discrepancy appears to be resolved in the 'constrained' model of Schwiderski (1983), where a negative amphidrome at (32° S, 24° W) is accompanied by a positive one at (34° S, 43° W), reconciling the open-ocean régime with the northward progression up the coast of Brazil and with a marked fall in coastal amplitude in the region of 28°–30° S. However, all models agree in presenting a long trough of low amplitude between Ascension Island and south Brazil.

Cartwright (1971) attempted to locate a negative M_2 node by interpolating between (then) new tidal data from the islands of St Helena, Ascension, Trindade and Tristan da Cunha. A linear interpolation gave a node at (27° S, 20° W), somewhat similarly to the 'unconstrained' model of Pekeris & Accad (1969) even closer to the improved models of Accad & Pekeris (1978, figure 7). Syntheses of Poincaré waves fitted to the island data by Cartwright (1971) banished the node off the map in a southwesterly direction, but these depended on the artificial assumption of a constant depth of ocean. Our new pelagic stations in the South Atlantic are not very well positioned for learning more about the region in question, but it is worth trying another interpolation with the latest corrected constants for Trindade, improved constants for Tristan da Cunha, and our pelagic stations at T7 and Hotspur Bank Seamont (figure 4*b*). The cotidal lines sketched at the bottom of figure 4*b* correspond to a six-parameter quadratic interpolation between the M_2 constants from the above stations together with St Helena and Ascension.

The interpolation just includes a node within its area of plausibility, some 6° further south than the linear interpolation mentioned above, which was in any case partly based on inaccurate data from Trindade (see §2*c*), and about 5° west of Schwiderski's (1983) position. The corresponding node for N_2 is shown to be considerably further north, as it is in Schwiderski's (1981) model, and continuity in frequency suggests correctly that any node for S_2 must be either a long way south of the M_2 node or non-existent. In Schwiderski's S_2 map, both negative and positive nodes degenerate into a trough of low amplitude and rapid phase change. In terms of normal ocean modes, the S_2 tide has more contribution from modes of natural period 11.6 h and 11.4 h (Platzman 1984, figure 14), which do not have strong negative amphidromes in this area.

Figure 4*b* also shows linearly interpolated positions for the positive diurnal amphidromes at O_1 and K_1, based on St Helena, Tristan da Cunha and station T7. These are generally agreed among modellers, and Schwiderski (1981) gives much the same positions. The more eastern position for O_1 accords with the existence of a sharply tuned zero-point between O_1 and M_1 in the diurnal admittance at Simon's Bay, Cape Providence (Cartwright 1971).

The middle and upper panels of figure 4*b* complement the lower panels of figure 4*a* in showing profiles of amplitude H and Greenwich phase lag G of the dominant tides M_2 and S_2 along a line between Natal and the coast of west Africa at Guinea-Bissau. This is not the same as the Natal–Dakar line along which admittances are plotted in figure 3*b*, but it lies much closer to the pelagic stations T1–T4, and it includes the island of Fernando de Noronha. The only station that is noticeably off the line is T4 (St Peter and Paul Rocks); its harmonic constants were adjusted to values appropriate to the bracketed cross by linear interpolation between T4 and FP1. The constants are seen to plot smoothly between the measured positions in the top panel.

No values have been plotted at the northern termination of the line because the coastline of

PHILOSOPHICAL TRANSACTIONS OF THE ROYAL SOCIETY A MATHEMATICAL, PHYSICAL & ENGINEERING SCIENCES

Guinea-Bissau is very indented with islands and shallow channels and with indications of a local semidiurnal resonance in the estuary of the Rio Geba. Of twelve ports and terminals whose tidal constants are listed in the *Admiralty tide tables*, ten have M_2 amplitudes greater than 99 cm which clearly cannot be compared with the oceanic values shown in figure 4*b*. North of Varela (12.8° N, 16.6° W; $H = 67$ cm $- M_2$, 21 cm $- S_2$), coastal amplitudes settle back to values comparable with T1, but there are irregularities in phase associated with the mouths of large rivers until as far north as Dakar (14.7° N, 17.4° W). We consider the tidal constants at our shelf-break pelagic station T1 to be adequately representative of the oceanic régime off this part of the African coast.

(*c*) *Semidiurnal anomalies*

As was first noted by Munk & Cartwright (1966), the semidiurnal tidal signal at any place consists not only of a lightly transformed representation of the gravitational potential in that frequency band according to a linear admittance function as discussed in §3*a*, but it also contains some anomalous effects that are strongly correlated with but of different physical origin than gravity. The 'radiational' input at S_2 is obvious from the trend of phase lag with frequency in most lists of harmonic constants. Phase lag generally increases with frequency through $N_2 - M_2 - K_2$, but the phase lag of S_2 is nearly always greater than that of K_2, though of slightly lower frequency than K_2. There is also an anomaly in the amplitude of S_2 compared with the amplitude of the gravitational potential, and a relatively smaller, though detectable radiational anomaly in K_2 itself.

Another type of anomaly results from nonlinear friction, producing triple-interaction harmonics at frequencies $(M_2 + M_2 - X_2)$, where X_2 is any primary semidiurnal harmonic. The compound frequencies also coincide with other, linearly generated harmonics, and the combined harmonic should conspire to reduce the total amplitude of motion when X_2 and M_2 come into phase, as pointed out by Garrett (1972). $X = S$ and $X = N$ are the most well-known contributors to this effect.

Both the above anomalies require at least a year of data to resolve with adequate approximation, so direct knowledge of their character has hitherto been based exclusively on coastal records. It has sometimes been suggested that they are merely local effects of shallow water, or land–breeze régimes. The seven one-year pelagic records detailed in table 1 give an opportunity to see how far the anomalies exist in the open ocean. Our procedure for extracting them from the data is outlined in §2(*d*).

Table 3 lists the total S_2 harmonic and its anomalous (non-gravitational) part for the seven pelagic stations and for sixteen other coastal and island ports in various regional groupings of interest. Only results from good data series, in some cases of several years' extent, are shown. The last two columns are the most important, giving the ratio and phase lag of the radiational harmonic (the anomaly) relative to the gravitational harmonic (total S_2 minus anomalous S_2). The ratios are reasonably consistent with each other and with similar results by Cartwright (1968) for the U.K. coast and by Zetler (1971) for the U.S.A. coasts. Zetler (1971) records a ratio of only 0.05 for Atlantic City, but our result is based on a much longer data series. There is nothing to suggest that the anomaly at pelagic stations is any different from the others. Where notably large or small values appear they appear to be regionally consistent. Thus, FP1–3–4 show an increasingly large ratio eastward along the Equator, but the value for FP4 is matched by Pointe Noire on the African coast, and nearby islands of Ascension and Fernando de

Table 3. Radiational anomalies at S_2

type	station	latitude deg N	longitude deg W	total S2 H	total S2 G	anomaly H	anomaly G	rad.:grav.	phase lag
mid-latitude pelagic	YN	57	10	39.3	202	4.4	338	0.1036	220
	YP	51	13	34.9	154	4.2	301	0.1093	210
	Y1	45	16	29.2	121	2.5	267	0.0794	211
	Y2	34	29	15.1	060	0.9	204	0.0573	216
equator pelagic	FP1	0	20	18.5	231	2.5	355	0.1259	229
	FP3	0	10	11.2	188	1.7	298	0.1447	243
	FP4	0	−6	16.7	126	3.4	240	0.1836	236
tropical coasts, islands	Natal	−6	35	27.9	232	3.4	355	0.1128	231
	Fernando	−4	33	25.8	227	3.1	358	0.1102	224
	Ascension	−8	14	11.8	201	1.9	326	0.1449	228
	Pointe Noire	−5	−12	16.8	113	3.6	250	0.1839	216
eastern coasts	Reykjavik	64	22	51.2	220	5.3	353	0.0964	224
	Valentia	52	10	40.8	155	4.4	296	0.0986	215
	Lagos	37	09	35.5	083	3.3	212	0.0867	227
	Dakar	15	17	16.6	293	1.8	070	0.0977	210
western coast	St John's	48	53	14.5	360	1.4	125	0.0916	231
	Atlantic City	39	74	12.1	018	1.5	193	0.1126	185
	Mayport	30	81	11.2	047	2.2	233	0.1634	175
other islands	Bermuda	32	65	8.1	024	0.9	185	0.1003	197
	Flores	39	31	13.7	078	1.0	203	0.0683	231
	Terceira	39	27	16.3	084	0.6	164	0.0349	277
	Madeira	33	17	26.8	067	1.4	184	0.0515	240
	S. Vicente	17	25	11.7	310	1.7	064	0.1363	239

Noronha have similar ratios according to longitude. The Azores islands of Flores and Terceira form another regional group with Y2, Madeira and perhaps Lagos, all showing subaverage ratios.

The phase lags in the last column of table 3 are remarkably consistent, grouped around 220° with the possible exception of Bermuda and the other two extreme western stations. Cartwright (1968 and other papers) has pointed out that a phase lag of 240° in the radiational S_2 tide relative to the gravitational tide would be consistent with driving by the atmospheric pressure tide whose minimum has a phase lag of 240° relative to local noon everywhere. Further, the static equivalent sea-water head of the S_2 atmospheric tide is nearly of form

$$1.24 \cos^3\theta \text{ cm}, \tag{4}$$

where θ is the latitude (Chapman & Lindzen 1970), and the solar gravitational tide potential is equivalent to

$$11.3 \cos^2\theta \text{ cm}. \tag{5}$$

Therefore the amplitude ratio at the Equator, 0.11, is quite in line with the ratios recorded in table 3, not incomparably low as has sometimes been suggested. As Zetler (1971) pointed out, the static ratio decreases with $\cos\theta$ away from the Equator, but some additional magnification may be introduced by the dynamic reaction to the different latitude factor in the driving force. Expressed differently, the atmospheric driving force will excite the same normal modes with natural periods around 12 h as the gravitational potential (5), but in different proportions according to their 'cross section' to the driving function (4) (Platzman 1984). The ratio of the

PHILOSOPHICAL TRANSACTIONS OF THE ROYAL SOCIETY A MATHEMATICAL, PHYSICAL & ENGINEERING SCIENCES

two responses will therefore be expected to have high spatial correlation due to the same modes being excited but some variability owing to their different weighting factors. This is in fact observed.

Anomalies due to nonlinear interactions of type $(M_2+M_2-X_2)$ were evaluated for the same stations as listed in table 3, but the results were too variable for any general physical deductions from them. Anomalous amplitudes corresponding to X = S and X = N were, except for a few coastal stations, generally less than 1 mbar and of order 0.1–0.3 times the total amplitude at the appropriate frequency, of similar magnitude at the pelagic as at the coastal and island stations. Interaction coefficients, relating the anomalous amplitude and phase to the amplitudes and phases of the supposed generating harmonics M_2 and X_2 were similarly too variable for generalization. It is possible that the splines used to interpolate linear admittance (1) were insufficiently accurate. The only broad conclusion is that the sought nonlinearities are too small in the deep ocean and at exposed coasts to be distinguished from noise; away from the inner reaches of continental shelves they may as well be neglected.

(*d*) *Fourth-diurnal tides*

It is sometimes suggested (e.g. Garrett & Munk 1971, footnote on p. 502) that fourth-diurnal 'overtides' like M_4, the first harmonic of M_2, may be an indicator of continental shelf friction, even at the low levels observed in the deep ocean. Energy is fed into such harmonics in every shelf sea, and they appear to obey their own laws of propagation independently of the primary tide; see for example the tidal maps for M_2 and M_4 in the North Sea computed by Davies *et al.* (1985). It may therefore be suspected that some of this energy is radiated into the deep ocean to provide a low-level background noise at high frequency. The relation to friction is not clear cut, because it is well known that harmonics are generated in shallow water wherever the ratio tidal elevations : mean depth is greater than about 10^{-1}, independently of frictional stress. However, frictional dissipation is roughly proportional to the cube of the tidal current which also tends to be large in inverse proportion to the depth (Davies *et al.* 1985, figure 5).

To give some idea of the relative magnitudes of second-harmonic energy to primary energy, in a shallow water area like the Southern Bight–eastern English Channel, the ratio of mean energy of M_4 to that of M_2 is about 10^{-2}. Because the effective mean friction in any tidal constituent is largely governed by the M_2 current speed, the ratio of the dissipation rates is only about 10^{-1}. The corresponding ratio of quality factor $Q = \omega E/\dot{E}$ is therefore of order

$$2\times 10^{-2}/10^{-1} = 0.2.$$

Thus, M_4 is more rapidly dissipated than M_2 within the shelf area.

When it comes to rate of energy transmission off the shelf, we may consider as a typical example the southwest approaches to the English Channel (Section j of figure 7*c* in C.E.S.V.). The average power flux along this 320 km section is 0.26 GW km^{-1}, into the shelf seas as one expects. The corresponding mean power flux associated with M_4 can only come from the product

$$\tfrac{1}{2}\rho g h u_n \zeta \cos\phi 10^{-3} \text{ GW km}^{-1},$$

where ρ, g are sea density and gravity, $h = 180$ m is the depth at the shelf break, u_n, ζ are current amplitude inwardly normal to the section and tidal amplitude, both for the M_4 constituent, and ϕ is their phase difference. From measurements of both current and elevation

at a typical point on this section, we find $\phi = 175°$, which confirms outward radiation as the only physically meaningful direction in this case, but u_n and ζ are about 0.07 and 0.012 times their corresponding values for M_2, so the power flux is of order 10^{-3} times the M_2 flux into the shelf sea. The relatively small amount of energy loss attributable to M_4 would appear to be dissipated on the shelf itself rather than radiated into the deep ocean.

Nevertheless, there is some scientific interest in what level of M_4 amplitude may be built up in the ocean. It is easy to extract by ordinary harmonic analysis, and Spencer & Vassie (1985) have reckoned that the second harmonic (unlike the third) can hardly arise from instrumental defects. Zetler *et al.* (1975) found amplitudes of order 0.07 mbar and coherent phases in very good instrumental records from the deep MODE area southwest of Bermuda. They observed that such values are more than an order of magnitude greater than one could expect from linear generation through the P_4 harmonic of the gravitational potential.

M_4 amplitudes and phases from our pelagic (off-shelf) records are listed with M_3 values in Appendix B. They are mostly confirmed by similar values from two independent pressure sensors, so they are unlikely to be instrumental artefacts. Unfortunately neither amplitudes or phases follow any recognizable spatial pattern, possibly because the free tidal wave at this frequency has structure too detailed for resolution by our array, a conclusion also reached for M_3 in §4*c*. Amplitudes are nearly all in the range 0.1–0.6 mbar, except from some higher values of 0.7–1.0 mbar close to the British shelf and in the Gulf of Guinea. Those west of the British shelf (for example YN, 0.79 and YP, 0.96 mbar) are probably an overspill from the local shallow areas. In the Gulf of Guinea (for example, FP3, 0.75 and FP4, 1.34 mbar) there is no effective local shallow region and the enhanced amplitudes are probably caused by internal tide motion of low stability in the strong density structure there (Cartwright *et al.* 1987).

There are some sequences of smooth progressions in phase along the lines of stations from the Azores to Newfoundland, from the mid-Atlantic Ridge to French Guiana (stations G1–G5), and from Natal to Dakar, all lines represented in figure 2. These are manifestly not directions of radiant energy from generating sources, and the phases are coherent over too great distances for an internal tide source. The phase progression must be a manifestation of the free-wave structure over the whole ocean basin. Whatever this wave structure is it is not the same as the M_2 structure. The amplitude of M_4 at B2 near the northern M_2 amphidrome is 0.36 mbar, about the same as at G5 where the M_2 amplitude is nearly 60 mbar. The amplitudes in the MODE area studied by Zetler *et al.* (1975) are with G2 (0.10 mbar) the smallest recorded values in the North Atlantic, but the M_2 tide there (34 mbar) is of average amplitude.

4. Long-period and third-degree tides

Before returning to the problem of mapping the principal diurnal and semidiurnal tides, we shall consider some tidal components of small amplitude but considerable oceanographic interest.

(*a*) *Long-period tides in the tropical Atlantic*

Much effort has been devoted to extracting the monthly (Mm) and fortnightly (Mf) components of Pacific and Indian Ocean tides and assessing their closeness to 'equilibrium' (Wunsch 1967; Agnew & Farrell 1978; Luther 1980). Cartwright (1968, 1983) found near-equilibrium values at some British stations, but apart from this little interest has been shown

PHILOSOPHICAL TRANSACTIONS OF THE ROYAL SOCIETY A MATHEMATICAL, PHYSICAL & ENGINEERING SCIENCES

in Mm and Mf in the Atlantic Ocean, perhaps because all its long tidal records (excepting monthly mean sea levels, which are obviously useless for this purpose) are from the midlatitudes where noise level is high. A long series from the subtropical station at Simons Bay, South Africa was shown by Cartwright (1971)† to have its Mm and Mf content below noise level because of proximity to the zero of the function

$$(1-3\sin^2\theta),$$

which describes the latitudinal dependence of the zonal tide-raising potential.

Mm and Mf turned out to be surprisingly prominent in our 18-month series at FP1, FP3, FP4 along the Equator, partly because of a low noise level. Even the nine-day tide, sometimes called Mt, proved to be detectable at about 0.5 mbar amplitude, as also found by Luther (1980) in tropical Pacific records. We then looked at other fairly recent sea level records from the tropical Atlantic and found that they too contained Mm and Mf signals significantly above noise level in 1 year records. A summary of amplitudes, phase lags, admittance ratios R and their standard errors r, from ten stations is given in table 4.

TABLE 4. ADMITTANCES FOR Mm AND Mf

station	latitude deg N	longitude deg W	unit	H (Mm)	$G°$	R, r	H (Mf)	$G°$	R, r
Natal	−6	35	cm	—	—	—	1.6	17	1.06, 0.37
Fernando	−4	33	mbar	1.1	10	1.4, 0.5	1.7	03	1.11, 0.20
SPPR	1	29	mbar	1.1	20	1.3, 0.4	1.9	−07	1.21, 0.15
Ascension	−8	14	mbar	0.7	−04	0.9, 0.4	1.9	−02	1.28, 0.15
FP1	0	20	mbar	1.1	02	1.3, 0.2	2.1	−05	1.35, 0.08
FP3	0	10	mbar	1.0	−08	1.2, 0.3	2.1	−05	1.37, 0.22
FP4	0	−6	mbar	1.1	13	1.4, 0.2	2.1	−05	1.41, 0.09
São Tomé	0	−7	mbar	1.1	13	1.4, 0.4	2.2	−24	1.49, 0.25
Annobon	−1	−6	mbar	0.9	−34	1.2, 0.4	2.1	−09	1.42, 0.25
Pointe Noire	−5	−12	cm	—	—	—	1.5	49	1.04, 0.40

Standard errors r were estimated from nearby spectral levels; multiplying by 57° (1 rad) gives approximate error levels for phase lag G. Absence of figures implies insignificant signal:noise ratio. One year pressure records from Fernando de Noronha, St Peter and Paul Rocks (SPPR), São Tomé and Annobon were kindly supplied by J.-M. Verstraete of ORSTOM (France).

Admittance ratios were calculated by dividing amplitudes H by the 'self-consistent equilibrium tide' computed by Agnew & Farrell (1978). This is a refinement of the classic potential form adjusted to allow fully for self-attraction of the realistically shaped ocean crustal yielding including the loading effect. Figures were read to one decimal place from the map (figure 1) and formula of Agnew & Farrell (1978) and the sum was then multiplied by the known harmonic amplitudes of the external gravitational potential. Effectively, this procedure replaced the usual constant elastic factor $(1+k-h)=0.69$ by factors dependent on geographical position with values between 0.68 and 0.75 in the area concerned.

With little more than a year of data from each site one cannot expect precise estimates of

† An anomalous monthly tide attributed by Cartwright (1971) to the third-degree potential was later found to be undetectable in the following nine years of data at Simons Bay and at Port Nolloth (RSA).

PHILOSOPHICAL TRANSACTIONS OF THE ROYAL SOCIETY A MATHEMATICAL, PHYSICAL & ENGINEERING SCIENCES

admittance, but the listed values of R are surprisingly consistent over the area, with phases differing insignificantly from the 'equilibrium' value zero in both Mm and Mf. R values are mostly greater than unity, a distinctly non-equilibrium feature. In the case of Mm, having larger noise ratio, some excess will be attributable to positive sampling bias; a bias-free estimate would be

$$R' = (R^2 - r^2)^{\frac{1}{2}}$$

but this is mostly only about 0.5% less than R, much less for the Mf estimates. As far as one can interpret such noisy estimates statistically, there seems to be evidence for amplification at both frequencies, with the Mf values tending to increase eastwards. Luther's (1980) estimates of admittance amplitude at Mf from data of many years at Pacific islands are mostly less than unity with a few exceptions. We cannot account for these differences between Atlantic and Pacific, but merely record them as apparently significant departures from the static tide even after allowing for all the physical adjustments in Agnew & Farrell's theory. (Use of a constant elastic factor 0.69 would make our R values even larger.)

The smooth progression in Mf amplitude from west to east does not support Wunsch's (1967) hypothesis of high-wavenumber Rossby modes. Luther (1980) also failed to find such short-scale structure, and attributed Wunsch's variability to sampling errors. However, some of the apparent smoothness in our results may be due to much of our data being simultaneous. Schwiderski's (1982) map of the Mf tide, computed from coastal data with the conventional potential, also increases slightly from west to east but with typical amplitudes in the range 1.8–2.0 cm, some 5% less than our observed amplitudes. His phase lags are all positive; ours are mostly negative except at the two coastal stations, Natal and Pointe Noire.

(*b*) *Third-degree tides*, M_1

The Atlantic Ocean exhibits a spatial antiresonance to the common diurnal potential proportional to

$$\gamma^2 \sin 2\theta \exp[\mathrm{i}(\lambda + \lambda_G - \lambda_M)],$$

where γ is the moon's parallax, θ is north latitude, and λ, λ_G, λ_M are east longitude and the right ascension of Greenwich and the Moon respectively. But it resonates strongly to the much smaller third degree potential proportional to

$$\gamma^3 \cos\theta (5 \sin^2\theta - 1) \exp[\mathrm{i}(\lambda + \lambda_G - \lambda_M)].$$

The two potentials have the same form in longitude (and time) but are respectively anti-symmetric and symmetric in latitude with respect to the Equator. The effect is most noticeable in the region of the frequency of M_1, one cycle per lunar day, where the third degree potential has its largest harmonic line and the lines of slightly different frequency associated with the main potential are themselves fairly weak. The synodic time for separation of these lines at and near M_1 is about 9 years, so the effect is only detectable from fairly long data series.

Cartwright (1975, 1976) showed that at several western European ports the third degree M_1 line was considerably greater in amplitude than the larger second degree line (also known loosely as M_1 or NO_1 but preferably M_1'), representing a ratio of third degree:second degree admittance of order 10. Platzman (1984) confirmed Cartwright's surmise that the normal oceanic modes near M_1, especially the one with natural period 25.7 h, were strongly excited

by the third-degree potential, and the cross section of the second degree potential weighted the 28.7 h and 21.2 h modes which have weak amplitudes in the Atlantic. He also showed similar differentiation between the ocean's response to second- and third-degree semidiurnal potentials, but because the second-degree tides have mostly quite large amplitudes, the third-degree semidiurnal response is more difficult to detect in observations.

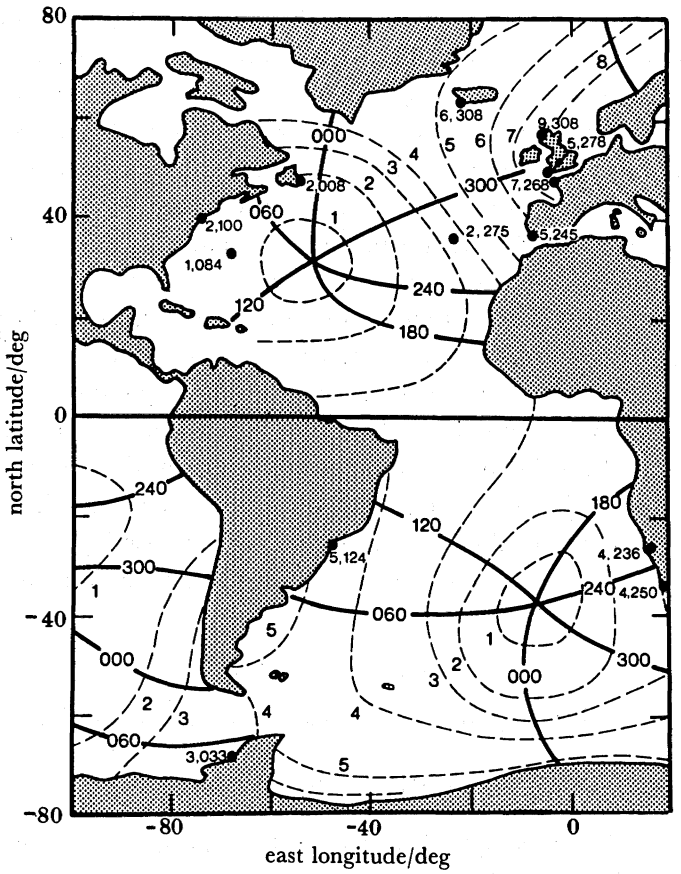

FIGURE 5. Contours of equal amplitude (millimetres, dashed lines), and equal phase lag (degrees, full lines) synthesized for the component M_1, transposed from figure 9 of Platzman (1984) with 60° arbitrarily added to phase values. Black circles are positions of multiyear coastal stations at which M_1 has been directly evaluated, with (amplitude, phase) shown.

We present in figure 5 the results of extracting the third degree M_1 component from a wider range of Atlantic stations than was available in Cartwright (1975, 1976). The 13 stations indicated by black spots with pairs of figures representing amplitude (in millimetres) and Greenwich phase lag (in degrees) are, in clockwise order from the furthest south, bracketed numbers giving years of data analysed: Faraday Base, Antarctica (9); Cananeia, Brazil (18); Bermuda (9); Atlantic City, U.S.A. (18); St John's, Newfoundland (9); Reykjavik, Iceland (9); Stornoway, Outer Hebrides (9); Newlyn, Cornwall (54); Brest, France (18); Terceira, Azores (5); Lagos, Portugal (9); Port Nolloth, RSA (9); Simons Bay, RSA (18). Cartwright (1975) also lists results from three stations in the North Sea. We are grateful to many national tidal authorities for the nearly two million data values supplied. All analyses were carried out

at IOS, including a 'response' analysis of the Cananeia data performed at Bidston by Dr J. Harari of the Universidade de São Paulo.

The contours on figure 5 are reproduced from Platzman's (1984) synthesis of the M_1 tide (his figure 9) by the sum of about ten normal modes of the world ocean, weighted according to their cross sections to the third degree diurnal potential and by a function of the differences of their natural frequencies from the lunar frequency. The broken contours are of amplitude (in millimetres); the continuous lines are cophase lines at 60° intervals. We have arbitrarily added 60° to the phase notation in Platzman's diagram because that adjustment gives better, in fact fairly good, agreement with most of the measured phases. The amplitudes are also in fair agreement with the contours, including the particularly large values around northern Europe and the very low values at Bermuda, Atlantic City and St John's. The slightly anomalous amplitudes at Newlyn and Stornoway are probably attributable to continental-shelf waves, discussed in relation to other diurnal tides in C.E.S.V. The general goodness of fit is considerably better than one based on the 25.7 h mode alone, especially in the region of Reykjavik.

We are unable to comment on the significance of our arbitrary 60° adjustment to the computed phases. An adjustment of similar magnitude but opposite sign would appear to be necessary to make Platzman's (1984) fit for M_2 agree with Atlantic coastal observations reasonably well. Platzman's modal wave forms are basically frictionless and do not allow for earth tide yielding, although friction is allowed for in a generalized way in forming his tidal syntheses. It must also be admitted that no computer simulation of the ocean tides which is not data-constrained has yet given an impressive degree of fit to data, and the phases appear to be particularly sensitive. One usually has to accept only qualitative agreement from this type of model, of which Platzman's is of course a unique variety, and on such a level the adjusted fit to data in figure 5 is remarkably good. There can be little doubt that the tidal map of M_1 is in fact fairly close to that depicted. We are unlikely to get any further data for this esoteric spectral line.

(*c*) *Third-degree tides*, M_3

The ter-diurnal spectral lines arising from the third-degree potential

$$\gamma^3 \cos^3\theta \exp\left[3i(\lambda+\lambda_G-\lambda_M)\right]$$

are no larger in amplitude than M_1 but they are much easier to extract from data series because of the absence of second-degree tides from that part of the spectrum. Nonlinear interactions such as (M_2+O_1) do not coincide with M_3 and are in any case negligible in this context.

In C.E.S.V. we presented a plausible tidal map for the main linear constituent M_3 in the northeast sector by hand drawing through a high-density array of pelagic and coastal data. We found that the present extended array did not permit us to do this with any conviction for the North Atlantic as a whole. There is evidence of fine structure which cannot be resolved in the neglected areas, and the coastal data apart from a few well studied stations are too contaminated by noise. Huthnance (1980) showed that local resonances with very high magnification were possible at this frequency, in particular along part of the south coast of Brazil. Such features clearly hinder extrapolation to the deep ocean.

Figure 6*a* shows the amplitudes (0.1 mm) at all pelagic and island stations. Apart from the three zones of amplitude less than 1 mm, which are ringed, and some tendency to increase towards coasts, it is hard to assign an overall pattern. The ringed areas are probably

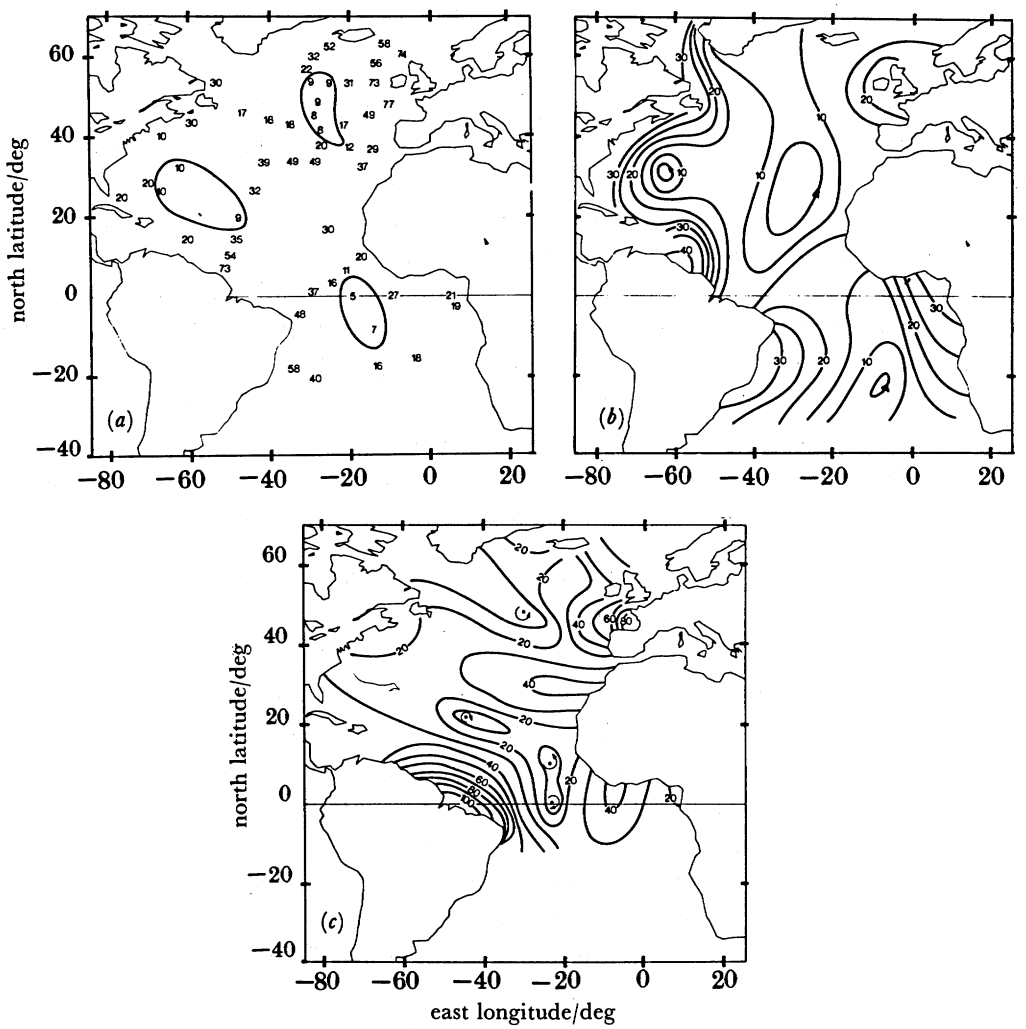

FIGURE 6. (*a*) Pelagic M_3 amplitudes in units of 10^{-2} mbar (or 1 Pa) or the nearly equivalent 10^{-1} mm for islands where elevation is measured directly. Closed contours mark zones of less than 10 units amplitude, possibly amphidromic. (*b*) A rough synthesis for co-amplitude contours of the M_3 tide computed from normal oceanic modes by formula (7). Units are the same as in (*a*). Arrows denote the sense of progression of phases round amphidromic centres. (*c*) A synthesis for co-amplitude contours of the M_3 tide computed from 50 Proudman functions with empirically derived coefficients in the manner of Sanchez *et al.* (1985). Units as in (*a*). Arrows denote the sense of progression of phases round amphidromic centres.

amphidromic and indeed are associated with rapid changes in phase (Appendix B) but we were unable to draw a consistent cophase map.

No computer model has been run for the M_3 tide to our knowledge, but Platzman *et al.* (1981) have computed all the normal modes with natural periods down to 8.0 h, all of which are depicted in Platzman (1985). Mode number 69 has a natural period of 8.26 h (frequency 2.91 c d^{-1}), which is very close to M_3 at 8.28 h (2.984 c d^{-1}). However, our computations of the 'cross section' or 'spectral input coefficient' $\bar{a}_k$ (Platzman 1984) of each modal waveform to the P_3^3 driving potential showed that spatial resonance was much greater between 1.1 and 2.4 c d^{-1} than around 2.9 c d^{-1} where it appears to be declining. Figure 7 shows the amplitudes of $\bar{a}_k$ and of their product with the resonance function of frequency f,

$$\Phi(f) = [(1-f/f_k)^2 + (2Q)^{-2}]^{-\frac{1}{2}}, \tag{6}$$

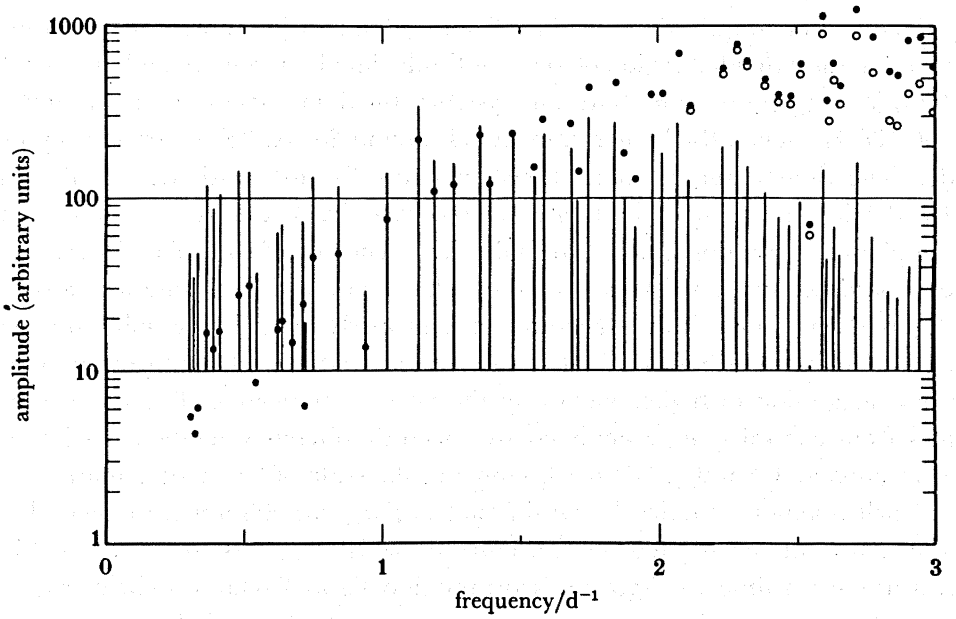

FIGURE 7. Vertical lines denote the amplitudes of the cross sections $\bar{a}_k$ of Platzman's normal modes of the world ocean to the P_3^3 harmonic of the tide-generating potential, with natural frequencies f_k corresponding to the horizontal scale (d^{-1}). Circles denote the products of $\bar{a}_k$ with $\Phi(f)$ (6) for the M_3 frequency ($f = 2.9841$ d^{-1}) and $Q = 10$ (full circles) and 5 (open circles). Where $Q = 5$ is not shown, its values are almost the same as for $Q = 10$.

where f_k is the natural frequency of mode k, and Q is an assumed 'quality factor'. Results are shown for $Q = 10$ and 5; the difference is negligible below $f = 2.0$ c d^{-1}. Platzman (1984) found $Q = 10$ gave the best compromise for M_2, but a lower value is probably most appropriate for M_3 because of its higher frequency and the dependence of its dissipation on semidiurnal currents. The greatest overall response is evidently in mode numbers 65 (2.72 c d^{-1}) and 61 (2.59 c d^{-1}), but many others contribute at a slightly lower weight including possibly some uncomputed modes above $f = 3$.

Both modes 65 and 61 contain much fine structure as expected, with about five positive amphidromes in the North Atlantic alone. For a more appropriate picture than either of these individually we computed the combined response of all modes,

$$\zeta(x, y) = \sum_k \Phi(f)\, |\bar{a}_k|\, H_k \exp\left[\mathrm{i}(G_k + \bar{c}_k + d_k)\right], \tag{7}$$

where $c_k = \arg(\bar{a}_k)$, $d_k = \operatorname{arccot}[2Q(1 - f/f_k)] > 0$, for $Q = 7$, and H_k, $G_k(x, y)$ are the arrays of normalized amplitude and phase lag for mode number k, which Professor Platzman kindly supplied to us on magnetic tape. The resulting tidal map defined by the complex array $\zeta(x, y)$ should be an approximation to the ocean's response to M_3, with limitations due to the lack of modes $f_k > 3$ and the oversimplification of (7).

Because of the fine spatial structure and the uncertainty about the modelled phase mentioned in connection with other constituents in §4*b*, we were unable to relate $\zeta(x, y)$ directly to the data or find better agreement with other values of Q, but the map of the amplitude field $|\zeta|$ shown in figure 6*b* shows sufficient points of qualitative similarity to have some interest. We note first that the general range of amplitudes are of similar magnitude to the data in figure 6*b*. Coastal amplitudes tend to be greater, but many of them are probably positively biassed by noise, and Platzman's model ocean does not strictly extend into continental shelf seas.

PHILOSOPHICAL TRANSACTIONS OF THE ROYAL SOCIETY A MATHEMATICAL, PHYSICAL & ENGINEERING SCIENCES

The large lobe of low amplitude extending from Iceland to just north of the Equator is probably related to the extended region of low amplitude data between Iceland and the Azores for which C.E.S.V. assigned two amphidromic systems; the data suggest another amphidrome near 20° N, 50° W. However, the higher data values around 35° N, 35° W are not reproduced by the model. The tighter amphidrome shown in figure 6*b* just south west of Bermuda is supported by the low amplitudes in figure 6*a* recorded by Zetler *et al.* (1975), but the corresponding phase distribution is not clear in the data. The other large lobe of low amplitude south of the Equator at about 10° W is probably related to the ringed zone which spans the Equator in figure 6*a*, without all the structure being properly modelled. Finally, the maxima approaching the Guiana and South Brazil coasts are reasonably well supported by the data, while there is a suggestion of higher values on the north American shelf. Among the more reliable values from coastal gauges analysed by spectral coherency methods, Atlantic City (40° W) has 53 units and Natal (6° S) has 65 units in the scale of figure 6; Cananeia (24° S) in the zone of shelf resonance studied by Huthnance (1980), has 693 units. In general, unlike the broader structure of the M_1 harmonic (figure 5) which appears to be reasonably well modelled, even at the coastline, by Platzman's formulation, figure 6 is far from being a definitive map of M_3 amplitude, but it has some resemblances to the measured data and provides a plausible alternative to the hopeless task of drawing adequate contours through the sparse data array. Phases remain confused in both data and model. If the M_3 tide is to be modelled more convincingly a much finer numerical grid would be required. Most of the coastal data is probably too noisy for Schwiderski's (1980) approach; the present pelagic data would provide a sounder basis of constraints, at least in the North Atlantic Ocean.

Figure 6*c* shows the result of a different sort of attempt to model the M_3 tide, by using an orthogonal set of 'basis functions' as proposed by Sanchez *et al.* (1985). The basis functions, to be discussed at greater length in §5, were computed by Dr D. B. Rao of the United States (NOAA) National Meteorological Center, using a three-degree grid covering the entire Atlantic–Indian Ocean area. Each member of the set conserves mass and prohibits flow across the external boundaries (mostly coastlines), but embodies no dynamic constraints. The essential difference between this approach and that of figure 6*b* is that here we have adjusted the coefficients of a relatively large number of functions to fit the empirical data by least squares, whereas the synthesis (7) of normal modes was not at all constrained empirically. All pelagic data and a selection of coastal tidal constants from both ocean areas were used in the fitting process, but figure 6*c* maps the result only in the area of the Atlantic Ocean where the pelagic data are densest.

We used only the first 50 basis functions for M_3 as compared with 100 for M_2 (§5), because there seemed little prospect of obtaining a much better fit to the noisy coastal data. The r.m.s. residual error (after the data selection procedure to be described in §5 and the removal of data from areas of known local resonance such as the Brazilian shelf (Huthnance 1980)) was 4.5 mm, largely from coastal anomalies.

The resulting amplitude figure 6*c* is very different from 6*b*, but has some superficial resemblances in the zone of large amplitude off the north coast of South America and zones of low amplitude in most of the central parts of the ocean, although with some geographic displacement. Figure 6*c* correctly places a positive amphidrome north of the Azores (cf. C.E.S.V., figure 14) and a negative one near 22° N, 44° W, which is supported by one of our lines of pelagic stations. The synthesis does not reproduce the negative amphidrome just east

of the Azores postulated in C.E.S.V., or the positive amphidrome south of Bermuda which was suggested by the normal mode synthesis, figure 6*b*. A broad area of fairly low amplitude in the Bermuda region accords better with the data in figure 6*a*. The close pair of counter-rotating amphidromes between west Africa and Brazil, one of them on the Equator, again approximates to the observed data in that region.

Figure 14 of C.E.S.V. based directly on the data, shows a zone of higher amplitude rotating negatively round Iceland, rather like a trapped Kelvin wave. The absence of any corresponding feature in the present figure 6*b*, *c* is probably due to Iceland not being resolved in the model from which either set of basis functions was computed. The northern boundary of the model of Rao is also close to Iceland, giving artificial constraint in that region.

On the whole, the representation by fitted basis functions is closer to the pelagic data than the purely dynamical synthesis of normal modes, as one might expect. However, the erratic coastal data again prevents a really authentic representation.

(*d*) *Radiational tides of high degree*

We turn in this section finally to the solar tides at ter-diurnal and higher frequencies, which Spencer & Vassie (1985) showed to be prominent in the spectra of bottom pressures at low latitudes. Figure 8 shows a representative set of energy spectra of one year records at station Y2 (34° N, 29.4° W) before and after subtraction of a harmonic tidal synthesis and of a two-hourly record of atmospheric pressure at Ascension Island (8° S, 14° W). The frequency resolution of all spectra is of order 2 a^{-1}, so solar and lunar components are easily distinguished but not the fine 1 a^{-1} splitting in the solar tides. As well as showing the usual higher harmonics of the lunar tide at a low but distinguishable level, it is surprising to see also prominent lines at or near the solar frequencies labelled $S_3 \ldots S_{11}$. These stand out even more in the spectrum of the tidal residual (middle panel) because, except for S_2, these solar harmonics are not included in conventional tidal syntheses. All our yearly records (table 1) showed similar characteristics, but north of about 45° N the harmonics above S_4 tend to be submerged by the noise continuum.

The higher solar harmonics are well known to occur in the atmospheric tides, as the bottom panel of figure 8 confirms. They are due to the day–night discontinuity in the solar radiation received at any given place. Their appearance in the pressure signal at the bottom of the ocean shows that at these frequencies the ocean responds to the global atmospheric signals in a non-static way, as we should expect from our previous consideration of the radiational content of S_2 (§3*c*). The same signals must therefore exist in the sea-level records from float-gauges, where the much higher noise level accounts for their lack of attention. Only S_4 is commonly allowed for in surface tides, but as a possible nonlinear harmonic of S_2; in the present context the nonlinearity is in the atmosphere, not the ocean.

We have examined in some detail the fine spectral structure around S_3 as the largest of the anomalous solar lines shown in figure 8. Input from the gravitational potential is quite negligible here. Oceanic nonlinearity could conceivably contribute at the sum-frequency of S_2 and K_1 which is 1 a^{-1} greater than that of S_3, but not to S_3 itself which is precisely three cycles per mean solar day. Table 5 shows the amplitude in 0.1 mbar and 1 mm units at the frequencies corresponding to S_3 and $S_3 \pm 1$ a^{-1} at the Ascension atmospheric and ocean pressure stations, four 1 year deep pressure stations and four multiyear surface tidal sea-level stations. (The outer frequencies could be named SK_3 and SP_3 respectively but that connotation could

PHILOSOPHICAL TRANSACTIONS OF THE ROYAL SOCIETY A MATHEMATICAL, PHYSICAL & ENGINEERING SCIENCES

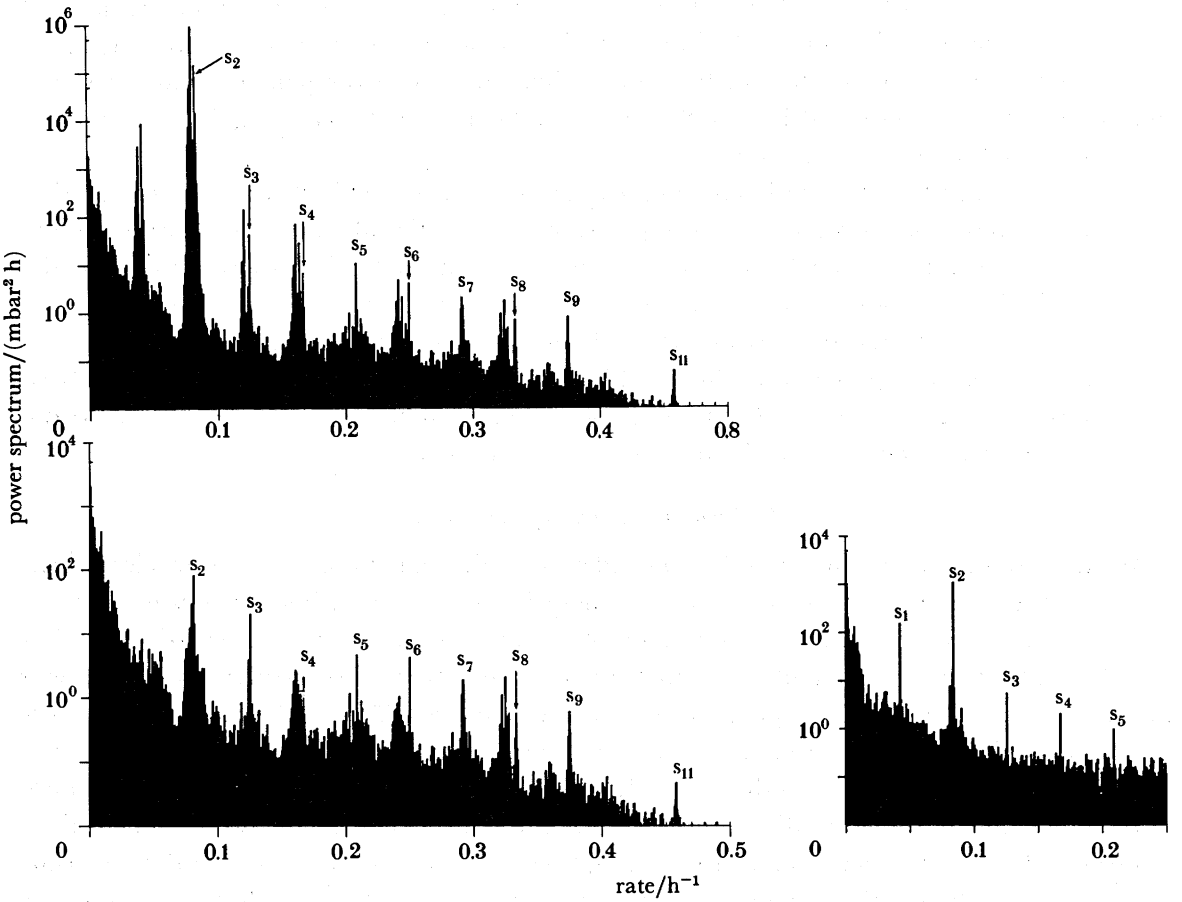

FIGURE 8. Top: the power spectrum of a one-year hourly bottom pressure record from position Y2 (34° N, 29° W), with resolution of $(4096\ \mathrm{h})^{-1} = 2.14\ \mathrm{a}^{-1}$; symbols denote solar spectral lines. Bottom left: spectrum of the same record after removal of a conventional harmonic tidal synthesis based on the gravitational tides. Bottom right: spectrum of a one-year record of two-hourly barometric pressure at Ascension Island.

imply lunar nodal modulations associated with K_1 and P_1, which would be inappropriate in that present context.) The three frequencies are only just resolvable in the one year records but their amplitudes are probably reliable on account of the low noise level. The surface stations were carefully analysed by spectral coherency averaged over many years to avoid noise-induced bias.

We see from table 5 that the oceanic bottom pressures are considerably larger than the atmospheric values at Ascension, but agree qualitatively with them in having somewhat larger and similar amplitudes at the two outside lines than at the central S_3 line. The coastal sea level stations by contrast have largest amplitude at S_3 and are mostly larger than the pelagic values in equivalent units, except for Bermuda which is comparable with the Ascension (shallow) ocean pressure record. Cananeia, from the region of the Brazilian coast with local shelf resonance to M_3 (Huthnance 1980), has greatly magnified values at these solar frequencies also.

The phase lags in degrees included in table 5 are referred to the same arguments as would apply to the combinations $S_2 + P_1$, $S_2 + S_1$, $S_2 + K_1$ in conventional harmonic analysis, including the 180° increment to the phase of P_1 to allow for a change of sign in its equilibrium amplitude.

TABLE 5. TER-DIURNAL SOLAR AMPLITUDES AND PHASE LAGS

station		units	$S_3-1\ a^{-1}$	S_3	$S_3+1\ a^{-1}$
Ascension	atmosphere	0.1 mbar	0.4, 343	0.2, 028	0.5, 307
Ascension	ocean	0.1 mbar	1.9, 050	0.1, 313	1.5, 042
Y2	ocean	0.1 mbar	1.5, 152	1.0, 136	1.5, 143
FP1	ocean	0.1 mbar	1.8, 074	1.2, 299	1.5, 065
FP3	ocean	0.1 mbar	1.1, 051	0.8, 292	1.4, 037
FP4	ocean	0.1 mbar	2.1, 327	1.5, 067	2.2, 325
St John's	sea level	mm	4.1, 229	7.9, 276	3.4, 241
Atlantic City	sea level	mm	1.6, 291	5.9, 288	1.4, 305
Bermuda	sea level	mm	0.1, 047	0.9, 215	0.2, 010
Cananeia	sea level	mm	8.2, 079	20.4, 264	10.0, 088

The general picture is that the phase lags at $S_3 \pm 1\ a^{-1}$ are, like their amplitudes, very similar to each other, as if these terms were driven by the same potential of similar structure. The phase lags of S_3, however, appear to be unrelated to those of the outside terms, as if due to a different generating mechanism.

These results lead us to consider the structure of the radiational input in the ter-diurnal band. A 'radiational potential' was defined by Munk & Cartwright (1966) as

$$\Psi = S(\xi/\bar{\xi})\,\nu\cos\alpha \quad \text{for} \quad 0 < \alpha < \tfrac{1}{2}\pi, \quad 0 \text{ otherwise}, \tag{8}$$

where S is the solar constant of radiation, taken here as unity, ξ is the Sun's parallax and $\bar{\xi}$ its mean value, ν is the ratio of the Sun's distance from the Earth's centre to its distance from a surface point $P(\theta,\lambda)$, and α is the Sun's zenith angle at P. $\Psi = 0$ corresponds to night-time. Ψ may be expressed continuously by expansion in Legendre polynomials as

$$\Psi/S = (\xi/\bar{\xi})\,[\tfrac{1}{4}+\tfrac{1}{2}P_1(\cos\alpha)+\tfrac{5}{16}P_2(\cos\alpha)-\tfrac{3}{32}P_4(\cos\alpha)+\ldots+O(\xi)]. \tag{9}$$

Here the P_1 term accounts for an annual cycle (S_a) and a daily cycle (S_1), but all higher odd-order terms $P_3, P_5 \ldots$ are of order $\xi \approx \frac{1}{60}$ and are therefore ignored in comparison with the even-order terms.

Each of the terms $(\xi/\bar{\xi})\,P_n(\cos\alpha)$ in (9) may be further expanded in a harmonic series

$$\sum_{m=0}^{n} C_{i,m,n} \sin\left(k_1^{(i)}\phi_1 + k_2^{(i)}\phi_2 + k_3^{(i)}\phi_3\right) Y_n^m(\theta,\lambda), \tag{10}$$

where ϕ_1 is the celestial longitude of the Greenwich meridian, ϕ_2 is the Sun's mean longitude, ϕ_3 is the Sun's mean perigean longitude, k_1, k_2, k_3 are associated small integers, Y_n^m is the normalized spherical harmonic of degree n, order m in geographical coordinates (θ,λ). The $C_{i,m,n}$ are numerical coefficients which may be evaluated by algebraic expansion of the elementary orbital equations for the Sun, neglecting powers of the eccentricity beyond the first. Even values of $(m+n)$ gave rise to the cosine terms, odd values the sine terms. Table 6 of Cartwright & Tayler (1971) lists the coefficients in (10) corresponding to P_1 and P_2 in (9), using the full lunar Doodson number

$$(l_1, l_2, \ldots, l_6) = (k_1, k_1, k_2, 0, 0, k_3).$$

For the present purpose, because the P_3 term in (9) is supposed negligible, the leading input to the ter-diurnal frequency band must come from the term in P_4. We have expanded this term

harmonically by the method outlined above. Orbital constants for epoch 1950.0 were used, namely 0.01673 for eccentricity and 23.445° for obliquity, for the sake of uniformity with table 6 of Cartwright & Tayler (1971); the changes in a century or so affect only the fifth decimal in the final coefficients. Table 6 (below) lists the coefficients of all terms greater than 0.00005 in tidal species 2, 3 and 4. Species 0 and 1 are unlikely to have any practical relevance.

TABLE 6. HARMONIC EXPANSION OF P_4 TERM W (9)

species 2				species 3				species 4			
$k^{(i)}$			$C_{i,2,4}$	$k^{(i)}$			$C_{i,3,4}$	$k^{(i)}$			$C_{i,4,4}$
2	−5	1	0.00168	3	−5	1	0.00418	4	−5	1	−0.00737
2	−4	0	0.02230	3	−4	0	0.05549	4	−4	0	−0.09788
2	−3	−1	−0.00131	3	−3	−1	−0.00325	4	−3	−1	0.00573
2	−3	1	0.00158	3	−3	1	−0.00202	4	−3	1	−0.00071
2	−2	0	0.03782	3	−2	0	−0.04833	4	−2	0	−0.01686
2	−1	−1	−0.00095	3	−1	−1	0.00121	4	−1	−1	0.00042
2	−1	1	0.00021	3	−1	1	−0.00006		—		—
2	0	0	0.02543	3	0	0	−0.00686	4	0	0	−0.00109
2	1	−1	0.00021	3	1	−1	0.00006		—		—
2	1	1	−0.00005		—		—		—		—
2	2	0	0.00199	3	2	0	−0.00030		—		—
2	3	−1	0.00008		—		—		—		—

The expansion in tidal species 2 is included in table 6 chiefly to show that its largest terms are in S_2 (2 −2 0) and K_2 (2 0 0), and these are unlikely to be disentangled from the other contributors to these terms. The other large term at (2 −4 0) or $S_2 - 2\ a^{-1}$ may be of interest as an indicator of the level of importance of the P_4^2 radiational input, since it is extremely weak in the expansion of P_2^2. However, cursory examination of spectra from real oceanic data suggests that the effect is small. The principal harmonic in species 4 is at S_4 (4 −4 0), and is likely to be confused in oceanic records with the nonlinear first harmonic of S_2.

Focusing on species 3 which is the most relevant to this study, we see that the P_4 harmonics are indeed split between $S_3 \pm 1\ a^{-1}$ (3 −2 0) and (3 −4 0), and S_3 is represented by two terms (3 −3 ±1) of an order of magnitude lower amplitude. (The latter terms are in fact modulators of the principal terms related to the ellipticity of the orbit.) The distribution of amplitudes is somewhat similar to that of the P_2^1 term from (9), Cartwright & Tayler (1971, table 6), including the difference in sign (or 180° phase difference) between the two leading terms. In the case of the diurnal radiation, however, there is an additional input at S_1 due to the P_1^1 harmonic in (9). The dominance of roughly equal terms at $S_3 \pm 1\ a^{-1}$ in the pressure spectra of table 5, together with their similar phase lags is therefore explained by table 6, but not the enhanced S_3 amplitudes in the coastal records or the non-trivial S_3 amplitudes in the pressures. Indeed, the anomalous phases in S_3 suggest that it is due to another physical mechanism not modelled by (8).

A likely contributor to S_3 in the coastal records is the response of the recorder mechanisms to irregular solar heating of its housing. The recording instruments were of early 20th century vintage, more noted for robustness and longevity than for fine precision. The disposition of windows and shade in their housing is likely to distort the smooth daily temperature curve assumed in the global radiation (8), and this could be translated through thermomechanical response to an irregular daily signal in the apparent sea level, doubtless with a rich high-

harmonic content. At the same time, this explanation cannot alone account for the very large S_3 amplitude at Cananeia. More generally, there is probably some irregularity in the daily thermal response of the sea itself, more marked in coastal waters but having a lesser effect on the ocean at large.

5. Spatial syntheses and energetics

(*a*) *The mapping problem*

We now return to the major diurnal and semidiurnal components of the tide, and consider how best to map them from the given spatial distribution of amplitudes and phases. This fundamental problem has been the subject of intermittent researches from the time of Whewell (1833) to the present day, with increasing degrees of sophistication. Four basic approaches have been developed:

(1) geometrical interpolation between data points;
(2) free dynamical models;
(3) dynamical models with data as boundary constraints;
(4) expansion by sets of basis functions.

Method 1, which includes hand-tracing, is effective only where the spacing between data points is much smaller than the scale of the tidal wave. Examples have already been given in §3*b*, and intelligent hand-tracing was used extensively in C.E.S.V., by Luther & Wunsch (1975), McCammon & Wunsch (1977), and in several historical precedents based on sparse data. The main limitation is lack of dynamic control on such essentials as mass continuity and boundary flow which limits accuracy in interpreting the map in detail.

Method 2, which attempts to reproduce the tides solely from the dynamical forces and the shape of the ocean, though the most satisfying method aesthetically, is hardly relevant in the context of this paper because it makes no use of empirical data except for the tuning of one or two frictional parameters. The best examples (e.g. Accad & Pekeris 1978; Zahel 1978; Platzman 1984) give only rough agreement with measurements.

Method 3, exemplified by Schwiderski (1980), compensates for imperfect physical representation by forced agreement with all known elevation data. Apparently, this procedure is mathematically rigorous only if some artificial adjustments are made to the conditions for boundary flow, and it is difficult to make proper allowance for crustal loading and gravitational self-attraction of the tidal wave. By definition, it is hard to find elevation data which do not agree perfectly with Schwiderski's maps, which were all computed by this method, but recent pelagic data in areas remote from the computational constraints do show varying degrees of inaccuracy (Woodworth 1985).

Mathematical completeness requires the ocean area considered to be either completely bounded by coastlines as in Schwiderski's (1980) global model, or to have open boundaries along which elevations or currents (i.e. gradients of elevation) are specified (Proudman 1944). Dr Roger Flather and his colleagues at Bidston have constructed an advanced model of the diurnal and semidiurnal tides in the northeast Atlantic, including crustal loading and realistic dissipation on the shelves, with open boundary conditions supplied by a combination of the C.E.S.V. data and Schwiderski's computations. (Paper in preparation; see Proctor & Wolf (1984) for a preliminary account.) This approach could now be extended to cover most of the North Atlantic Ocean, with open boundaries along our line of data stations from Natal to

Dakar and from Cartwright to Inishbofin (figure 4*a*, *b*). However, such computations are beyond the scope of the present work. Instead, we have investigated the possibilities of method 4.

Expansion of the tidal field in terms of a suitable set of spatial basis functions with coefficients determined by data fit is probably the best compromise. There are many possible sets of basis functions. Spherical harmonics have been used in the context of satellite altimetry (Mazzega 1985), but these require expansion to very high order to follow coastal detail and there is no guarantee of the equations of continuity and boundary flow being satisfied. At the other extreme of sophistication the set of functions generated by Parke & Hendershott (1980), also Parke (1982), sum to agreement with all continental (but not pelagic or island) coastal elevations for given harmonic constituents and satisfy frictionless dynamical equations which rigorously include crustal loading and self-attraction.

We have experimented with fitting a set of non-dynamical basis functions whose use in the objective analysis of any type of tidal elevation data was proposed by Sanchez *et al.* (1985), and to which we have already referred in §4*c*. They consist simply of the eigenfunctions (ϕ) of

$$-\nabla h \nabla \phi \tag{11}$$

subject to the condition

$$h\boldsymbol{n}\cdot\nabla\phi = 0 \tag{12}$$

around all boundaries, where $h(x, y)$ is the ocean depth at (x, y), ∇ is the horizontal gradient operator, ϕ is a velocity potential whose gradient $(-h\nabla\phi)$ is the irrotational part of the mass-transport vector, and $\boldsymbol{n}$ is the vector normal to the boundary, in principle the coastline. The transport vector also includes a solenoidal part defined by a stream function, which is irrelevant when only surface elevation (or pressure) are concerned.

By the continuity equation, (11) exactly equals the vertical velocity of the surface, which for a harmonic motion of given frequency is equivalent to the elevation field. Condition (12) ensures zero flow across coastlines. The eigenfunctions of (11) subject to (12) thus form a complete set of basis functions suitable for general expansion of the tidal elevation field over the ocean basins considered. They are orthogonal, but orthogonality is only of limited value when integrating over a partial area determined by a given data set. They are ordered by the parameter

$$\nu_j = (g\bar{H}\lambda_j)^{\frac{1}{2}}, \tag{13}$$

termed by Sanchez *et al.* (1985) the 'non-rotating frequency of oscillation', where λ_j is the jth eigenvalue of (11) and (12) and $\bar{H}$ is the mean depth. D. B. Rao and his colleagues have computed the eigenfunctions for $j = 1$–470.

The most attractive property of these basis functions is that, while satisfying continuity and boundary conditions, they embody no dynamic prejudice, and are therefore adaptable to a wide variety of dynamical force fields, including internal friction. As a disadvantage, they do not allow for energy transmission across boundaries which would be desirable when dissipative shallow seas outside the chosen boundary are ignored. The basic idea of such an expansion for the ocean tides was first postulated by Proudman (1917), and we shall for convenience call them 'Proudman functions' in what follows.

While this technique has already been successfully applied to the study of the tides of small basins such as Lake Superior (Sanchez *et al.* 1985), the method has yet to be extended to the

global oceans. However, as an intermediate step, Proudman functions have been calculated (by Dr D. B. Rao and co-workers) for the Atlantic–Indian Ocean basin by using a three-degree square grid, and with imposed boundaries at the Drake Passage, the Labrador Sea, the Norwegian Sea and Denmark Strait, the Indonesian Archipelago and at the 145° E meridian south of Australia. These unpublished calculations provide the basic set of Proudman functions with which to parametrize the tidal data from the Atlantic and Indian Oceans. The results will only be of value in the part of the Atlantic Ocean with which this paper is mainly concerned. A description of earlier computations of Proudman functions for the Atlantic–Indian oceans made with a 6° square grid can be found in Sanchez *et al.* (1986).

In principle, the functions can also be used to compute the normal modes of the Atlantic–Indian oceans which should comprise a smaller, and therefore more efficient, set of functions for tidal parametrization. So far this work has not been done with the present set of Proudman functions. However, alternative normal-mode calculations for the global ocean do exist already by means of finite-element discretization of the linearized primitive equations for a barotropic world ocean (Platzman *et al.* 1981), although at present the normal modes so calculated do not provide for such features as tidal dissipation or ocean-tide self-attraction and crustal yielding. The modes are calculated on an irregular 'geodesic' grid in which the spherical triangles between sets of three neighbouring grid points are approximately equal in area, with the average area of a grid triangle equal to that of a 4.54° square at the Equator. The Platzman normal modes show a reasonable correspondence to those calculated with the Sanchez *et al.* (1986) 6° grid.

(*b*) *Data sources and selection*

There are four main sources of tidal constants used in the fitting to data described below. These comprise:

(1) the tidal database of the International Hydrographic Bureau (IHB 1979);

(2) *the British Admiralty tide tables* (ATT 1986);

(3) compilations of pelagic tidal measurements (Cartwright *et al.* 1979; Cartwright & Zetler 1985) together with recent, unpublished pelagic data;

(4) published tidal measurements not so far included in the large datasets (e.g. Lutjeharms *et al.* 1985).

It is essential that selected coastal and island values represent as far as possible the tidal characteristics of the adjacent open ocean. Each measurement was therefore carefully examined for its suitability for inclusion in a global ocean dataset. This selection, which is necessarily somewhat subjective, resulted in the rejection of:

(*a*) all data from the NW European continental shelf in preference to the copious pelagic data from the nearby deep ocean;

(*b*) data from coastal canals, rivers and gulfs (e.g. the Amazon delta, Guinea-Bissau delta or Bay of Fundy).

Data from the various sources were grouped into 3° squares, corresponding to the grid used for the Proudman functions, and the real and imaginary components $H\cos G$ and $H\sin G$ averaged over the squares. Values from coastal areas that fall outside the grid, owing to its saw-tooth nature along a curving coastline, were assigned to the nearest neighbouring grid square in the event of that square not already containing tidal information. Altogether, averaged values of tidal amplitude and phase for the O_1 and M_2 constituents were calculated for 320 of

PHILOSOPHICAL TRANSACTIONS OF THE ROYAL SOCIETY A MATHEMATICAL, PHYSICAL & ENGINEERING SCIENCES

the 1915 grid squares of the Atlantic–Indian Ocean basin, whereas for the M_3 constituent (§4*c*) only 175 grid-squares contained usable data with the majority in the North Atlantic (figure 9). The resulting available dataset is clearly unequally distributed across the ocean and the fits described below will therefore contain a bias resulting from this unavoidably uneven data spread, with greatest weight and therefore best accuracy in the North Atlantic.

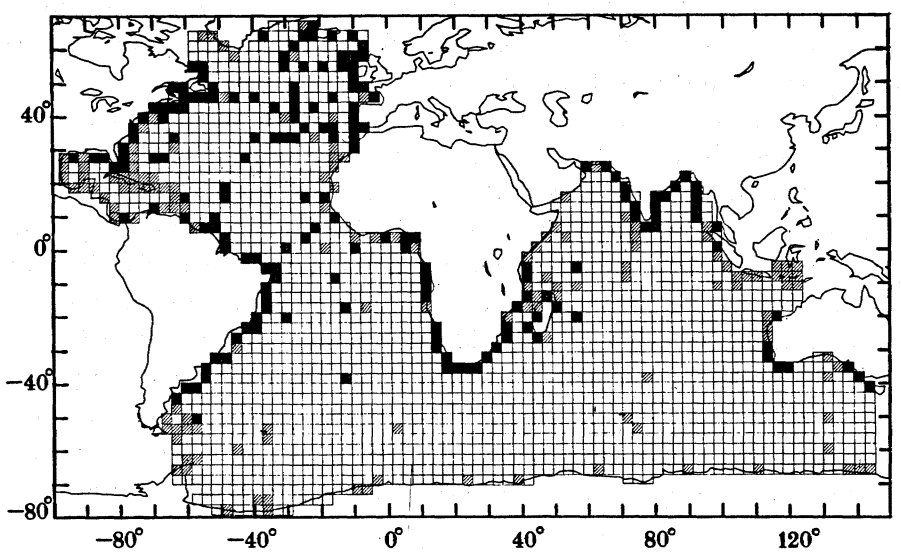

FIGURE 9. 3° square grid used for the calculation of Proudman functions. Hatched squares indicate selected O_1 and M_2 data; solid squares show selected O_1, M_2 and M_3 data.

It has to be recognized that not all local variability can be removed. Ideally one would like a network of pelagic tidal measurements off the continental shelf along each coastline together with measurements on an equally spaced grid across the deep ocean. However, such measurements are rare and one has to rely on data from stations in coastal locations which will have their own local peculiarities. In addition, the 3° grid will lead to averaging errors in areas where the tide varies rapidly.

(*c*) *Fitting by Proudman functions*

Following the analysis procedure of Sanchez *et al.* (1985), the tidal height field can be written

$$\zeta(x,y,t) = \sum_i a_i \phi_i(x,y) \cos\omega t - \sum_i b_i \phi_i(x,y) \sin\omega t, \tag{14}$$

where ω is the angular frequency of the tidal constituent in question, the $\phi_i(x,y)$ denote the Proudman function spatial distributions and the a_i and b_i are parameters to be determined by least-squares fitting to data. The amplitude, H, and phase lag, G, distributions are obtained by

$$H(x,y) = \sqrt{\{[\sum_i a_i \phi_i(x,y)]^2 + [\sum_i b_i \phi_i(x,y)]^2\}}$$

and

$$G(x,y) = \arctan\,[-[\sum_i b_i \phi_i(x,y)]/[\sum_i a_i \phi_i(x,y)]]. \tag{15}$$

Ideally one should use a smaller number of functions than data points to ensure a smooth fit. As the number of functions used approaches the number of data points, which represents an exact determination of the values a and b, the r.m.s. residual of the fit decreases towards zero (figure 10) but the overall tidal pattern in the basin, in areas where there are no data, deteriorates. A clear example of this effect is given in Sanchez *et al.* (1985). In their case, the

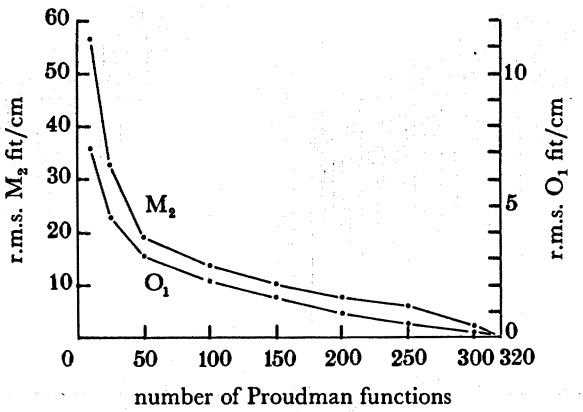

FIGURE 10. Root-mean-square residuals from parametrizations of O_1 and M_2 in terms of different numbers of Proudman functions.

optimum number of functions to be used in any objective analysis was estimated by comparison to the 'forced solution' for the basin. However, in the present study of the Atlantic–Indian Oceans with a 3° grid, a forced solution has not so far been computed, presenting a further subjective choice of the optimum number of functions to be used.

An estimate of the number of Proudman functions which will be required can be obtained by examining the coherence of each function with existing tidal models. One can define the area-weighted overlap

$$\text{overlap}_i = \frac{\int P_i H e^{iG}\, dA}{\sqrt{(\int P_i^2\, dA \int H^2\, dA)}} = c\, e^{id}, \tag{16}$$

where P_i is the spatial distribution of (real) Proudman function i and the integral is performed over the entire basin. Proudman functions that describe the major features of the tidal spatial distribution will have the largest values of c. Figure 11 *a*, *b* shows the values of c determined from the Schwiderski model plotted in terms of ν_j a parameter which is essentially inversely proportional to the typical wavelength of the function in question. Each constituent can be seen to be best described by the low-frequency, long-wavelength Proudman functions, O_1 more so than M_2, as one would anticipate from its broader scale. Consequently, the lowest Proudman function numbers, ordered in terms of frequency, are to be considered the most important for our purpose.

Figure 12 *a*, *b* present typical results of tidal charts for O_1 following parametrization of the data with the lowest-order 50 and 100 Proudman functions respectively. For figure 12 *a*, large amplitudes can be observed in the Southern Ocean and the Arabian Sea with low amplitude regions extending over most of the Atlantic and central-Indian Oceans. In many respects, the chart is very similar to that of Schwiderski (1981), although in this case the amphidrome in the

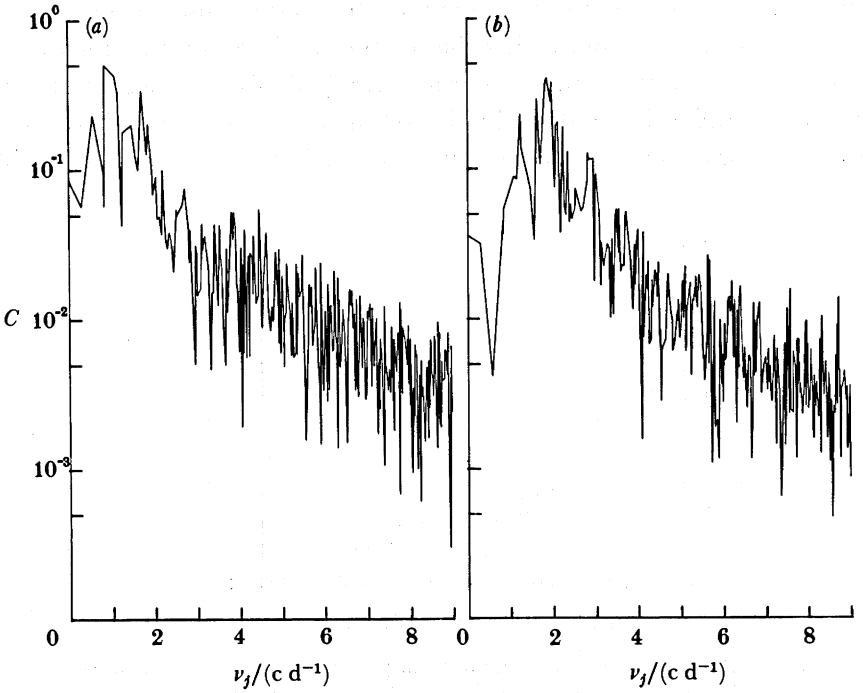

FIGURE 11. Overlap of the spatial distributions of Proudman functions with those of the Schwiderski model of the Atlantic and Indian oceans for (*a*) O_1 and (*b*) M_2.

south-west Indian Ocean is relatively displaced to the south-east by a small amount. The feature in the Atlantic significantly different to that in Schwiderski (1981) is the area around the Amazon mouth with phase lag larger than 240°; in the model the phase lag in this area is about 20° less. In fact, the fit of figure 12*a* merely reproduces the Brazilian values extracted from IHB (1979), most of which are larger than 240°. Data squares that contribute most to the r.m.s. residual error of 3.1 cm (i.e. residuals larger than 8 cm) comprise one square in the northern Caribbean (9 cm), three squares in the Antarctic peninsula–South Georgia area (9, 10, 15 cm), the square containing Heard Island in the southern Indian Ocean (13 cm) and three squares along the artificial model boundary to the north and south of Australia (8, 8, 10 cm). Increasing the number of fitted functions to 100 results in the beginning of the deterioration of the overall fit, as discussed above (figure 12*b*). Although the general amplitude pattern is maintained, the phase distribution distorts considerably, particularly in the low amplitude areas, as the fit begins to overconstrain the available data. At this stage, the accuracy of individual measurements in data-sparse areas becomes a critical factor. It appears, therefore, that approximately 50 Proudman functions are required to optimally describe the O_1 distribution in the Atlantic–Indian Ocean basin.

The fits to O_1 data demonstrate certain defficiencies with this sort of objective analysis. All fits to the tidal data will be biased towards areas where the tidal amplitude is large and rapidly changing at the expense of the large-area, low-amplitude regions, even though the empirical data for those areas may be well measured and even relatively copious. Therefore, although a fit to the available data may be adequate in an average sense, the quality of the tidal pattern in low-amplitude areas is often difficult to ascertain.

Figure 13 shows the corresponding tidal chart for the M_2 data using the lowest-order 100

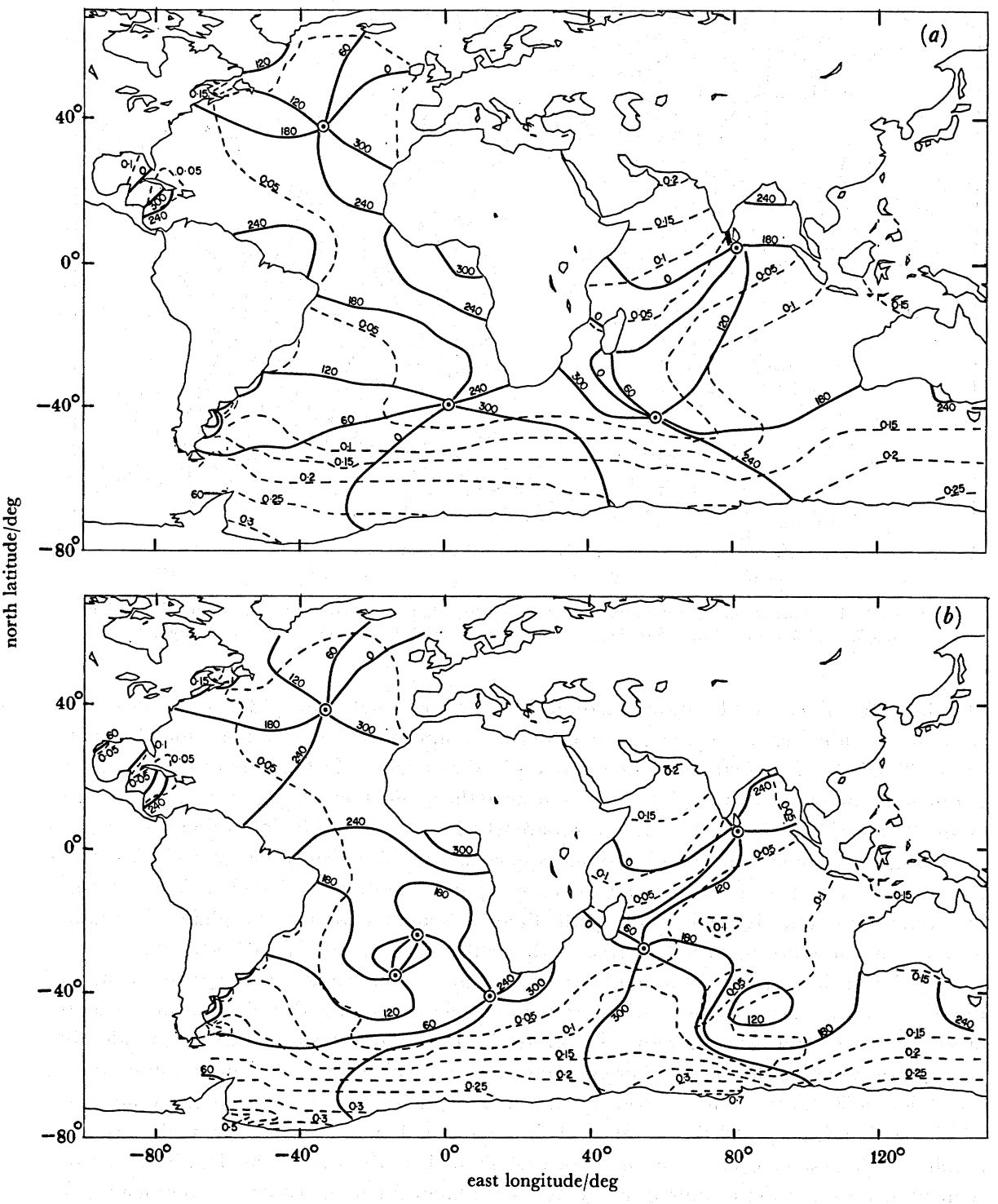

FIGURE 12. Tidal chart of the Atlantic and Indian oceans for O_1 parametrized in terms of (*a*) 50 and (*b*) 100 Proudman functions. Solid lines show phase lags in degrees and dotted lines show amplitudes in metres.

PHILOSOPHICAL TRANSACTIONS OF THE ROYAL SOCIETY A MATHEMATICAL, PHYSICAL & ENGINEERING SCIENCES

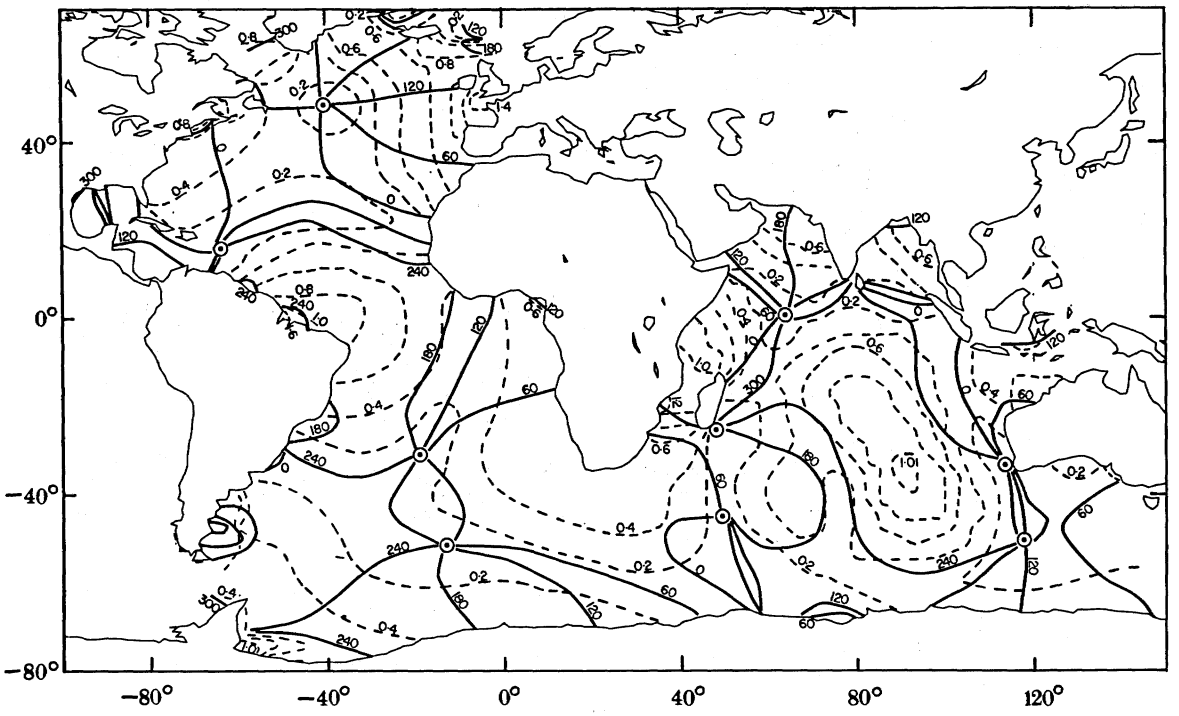

FIGURE 13. Tidal chart of the Atlantic and Indian oceans for M_2 parametrized in terms of 100 Proudman functions. Solid lines show phase lags in degrees and dotted lines show amplitudes in metres.

Proudman functions for the parametrization. The r.m.s. residual error is 13.8 cm. Data-squares with large residual errors (i.e. larger than 30 cm) comprise five squares along the Greenland coast (30, 37, 44, 50, 67 cm) and three squares in the Scotland–Iceland area (32, 36, 72 cm), both regions in which M_2 is rapidly varying near to the model boundary, as well as two squares on the Patagonian shelf (43, 44 cm), one square which includes the Gulf of Maine (37 cm), two squares off NW India (38, 67 cm) and one square to the NW of Australia (36 cm). A striking resemblance can be seen between this map for M_2 and that of Schwiderski (1983) in most of the Atlantic Ocean, although in the south there is a modification of the phase distribution which is known to be not entirely correct in the Schwiderski model (Woodworth 1985). In the Indian Ocean the existence of a number of important amphidromic systems at the corners of the ocean can be seen together with a large amplitude, anti-amphidromic area in the centre of the Indian Ocean. This pattern is qualitatively similar to but quantitatively considerably stronger than that deduced by other computer models, which show maximum amplitudes in the region of 50–60 cm. This is a consequence of the paucity of tidal information in the centre of the Indian Ocean. As the number of functions used in the fit is increased, this anti-amphidromic system becomes even more exaggerated as the overall fit deteriorates. Consequently, no more than approximately 100 Proudman functions can be recommended for parametrization of the M_2 tidal chart.

We have already discussed our attempt to fit the data from the M_3 tide in §4*c*. The poor quantity and quality of most of the data available for this constituent results in only 175 grid-squares being occupied and a correspondingly smaller justifiable number of Proudman functions, of which we chose the first fifty. The corresponding map, figure 6*c*, is only tentative.

(*d*) *Fitting by normal modes*

In §4*c* we attempted to synthesize the M_3 tide in the Atlantic by a filtered sum of normal modes of the world oceans as computed by Platzman *et al.* (1981). Success was only slight, largely on account of the lack of modes with frequency greater than 3 d^{-1}. The summation (7) was based on purely physical reasoning, without any recourse to empirical data, and so this approach was strictly of type 2 (§5*a*). We have also experimented with empirical fits of groups of Platzman's normal modes to the data for O_1 and M_2, thus treating the normal modes as a set of basis functions with arbitrary coefficients, as in approach 4. These functions differ from the Proudman functions in that they result from more sophisticated constraints to satisfy Laplace's tidal equations. The proper way of using their dynamical properties to model the tides is by the formulation of Platzman (1984), but treating the normal modes in a more empirical fashion does give promising results as shown by Woodworth & Cartwright (1986) in an analysis of satellite altimetry. Regrettably, our only concession to the physical meaning of the normal modes is to limit their natural frequencies to a small bandwidth of the frequency of the tidal constituent being fitted.

In principle, fewer normal modes than Proudman functions should be required to parametrize a tidal constituent to within a given accuracy providing that its Q is reasonably large (and, therefore, that its spatial distribution is dominated by a few near-resonant modes) and that the empirical data selected for fitting well represent the deep ocean tide. An estimate of which normal modes best match the shape of the ocean tide spatial distribution can be obtained by examining the coherence of each mode with a model in a similar fashion to (16) above. That is

$$\text{overlap}_i = \frac{\int P_i^* H e^{iG}\,dA}{\sqrt{\left(\int P_i P_i^*\,dA \int H^2\,dA\right)}} = c\,e^{id}, \tag{17}$$

where (17) is identical to (16) except that P_i now describes the complex normal mode i and P_i^* is its conjugate. Figure 14 shows the values of c for O_1 and M_2 determined from the Schwiderski model plotted in terms of normal mode frequency. Integration has been restricted to the Atlantic Ocean alone west of 30° E and within the common area of the Proudman and Platzman grids (i.e. essentially the Atlantic Ocean grid-squares of figure 9 minus the Caribbean). The importance of modes 16, 26, 33 and 39, in particular, in the Atlantic and Southern oceans has been emphasized above and in Platzman *et al.* (1981). In fact, from inspection of the *shape alone* of other normal modes with the Schwiderski (1981, 1983) distributions by means of published maps of the normal modes (Platzman 1985), it is quite evident why the other modes indicated in figure 14 have such large values of c if discussion is restricted to the Atlantic Ocean. For example, mode 17 has a rather similar *shape*, if not amplitude, to mode 16 in the Atlantic, whereas mode 31 (12.8 h), which one might have expected to be prominent from Platzman *et al.* (1981), has a relatively low value of c. (For convenience, we have used the mode numbering of Platzman *et al.* (1981), which is 15 less than that of Platzman (1985).)

In practice, an objective analysis of the empirical tidal dataset will not give similar results to figure 14, primarily because the available data are not geographically evenly distributed but also because the normal modes do not provide an orthogonal set of functions over a restricted ocean area such as the Atlantic. In fact one might expect to obtain a very similar total tidal pattern using different combinations of normal modes.

PHILOSOPHICAL TRANSACTIONS OF THE ROYAL SOCIETY A MATHEMATICAL, PHYSICAL & ENGINEERING SCIENCES

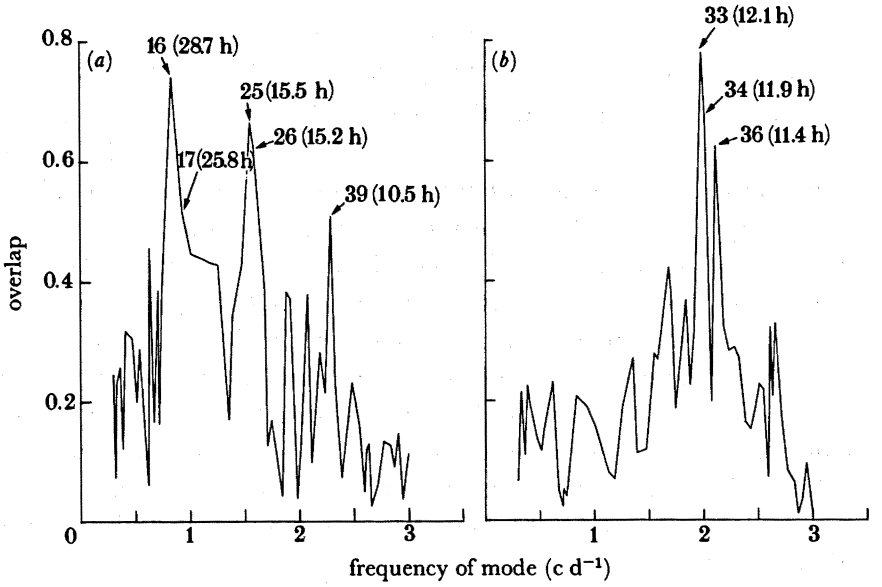

FIGURE 14. Overlap of the spatial distribution of Platzman normal modes with those of the Schwiderski model of the Atlantic Ocean for (*a*) O_1 and (*b*) M_2.

An objective analysis using normal modes differs from that with Proudman functions owing to the normal modes containing both amplitude and phase information. The real and imaginary parts of the tidal signal can be written

$$\left.\begin{aligned} H(x,y)\cos G(x,y) &= \sum_i v_i \Theta_i(x,y)\cos(\phi_i(x,y)-\Delta_i),\\ H(x,y)\sin G(x,y) &= \sum_i v_i \Theta_i(x,y)\sin(\phi_i(x,y)-\Delta_i),\end{aligned}\right\} \tag{18}$$

where Θ_i, ϕ_i are the amplitudes and phase lags for each normal mode i and the overall normalization and phase parameters, v_i and Δ_i, are obtained by means of least-squares fitting to the data.

A preliminary series of normal mode fits to O_1 and M_2 measurements in the Atlantic–Indian Ocean was by no means satisfactory, either qualitatively or quantitatively, as that which used Proudman functions. Several reasons can be found for this. Firstly, the geodesic grid used for the normal mode computations has a poorer spatial resolution at medium and high latitudes than the square-grid used to calculate the Proudman functions. This results in a considerably poorer description of the more complicated areas such as the Patagonian shelf and the NW Atlantic–Gulf of St Lawrence region. Secondly, there are simply fewer normal modes than Proudman functions available with which to perform a least-squares fit to a dataset which will always contain a geographically varying amount of non-oceanic tidal signal arising from small-scale coastal tidal variations and/or from measurement errors. To some extent this local variability is artificially absorbed in the Proudman function fits by the large number of free parameters used. Finally, there is the observation that the normal modes appear to give a somewhat better description of Atlantic than Indian Ocean M_2 (Platzman 1983, 1984) and the experience of Woodworth & Cartwright (1986) who found better fits to altimeter data by normal modes if each ocean was considered separately.

These considerations, together with the fact that empirical data from the central and southern Indian Ocean are extremely sparse, led to a series of fits of a small number of normal modes to O_1 and M_2 data for the Atlantic alone, with the Patagonian Shelf and St Lawrence regions removed in addition to the Caribbean which is not included by the simplified Platzman world coastline. Up to twenty modes were usually used in any one fit; if the syntheses described in Platzman (1983, 1984) are to be a guide then twenty should be sufficient for a description of Atlantic diurnal and semidiurnal tides.

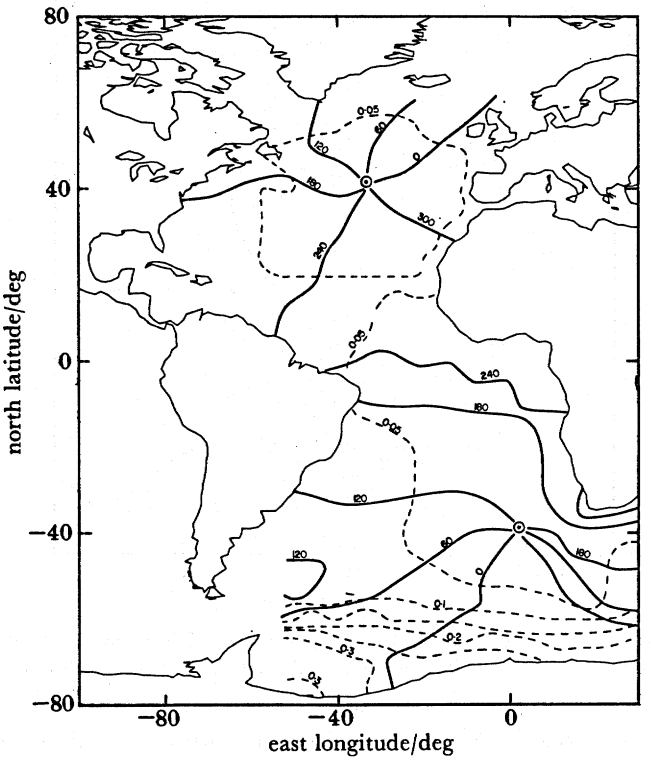

FIGURE 15. Tidal chart of the Atlantic Ocean for O_1 parametrized in terms of 20 Platzman normal modes. Solid lines show phase lags in degrees and dotted lines show amplitudes in metres.

Figure 15 shows the results of fitting a linear combination of twenty Platzman normal modes to Atlantic O_1 data. The modes chosen for fitting were numbers 7–26 of Platzman *et al.* (1981) (22–41 of Platzman 1985), with periods in the range 50.6–15.2 h with ten modes distributed either side of the O_1 period. The r.m.s. residual of the fit is a quite satisfactory 1.7 cm and the obtained spatial distribution well describes the major amphidromic features of the North and South Atlantic which are also suggested in several tidal models. Compared with Schwiderski (1981), it can be seen that once again there is a slightly larger phase lag obtained for the Amazon area, whereas in the South Atlantic there is some distortion of the low-amplitude area. This latter feature is poorly constrained by the complete absence of measurements from this part of the deep ocean. Reducing the number of modes used in the fit to 10 (modes 12–21 with periods 35.8–19.1 h) results in a marginally worse fit to the available data overall (r.m.s. = 2.2 cm) and virtually the same tidal pattern down to 30° S. The strong North Atlantic amphidrome appears as a stable feature in all fits. However, with the reduced number of modes a much poorer description of the low amplitude region of the SE Atlantic is obtained, and, in particular,

the phase progression of O_1 along the SW African coast is not reproduced in the fit. One concludes, therefore, that at least twenty normal-mode waveforms, more than anticipated, are required for a good objective analysis description of the available Atlantic O_1 data.

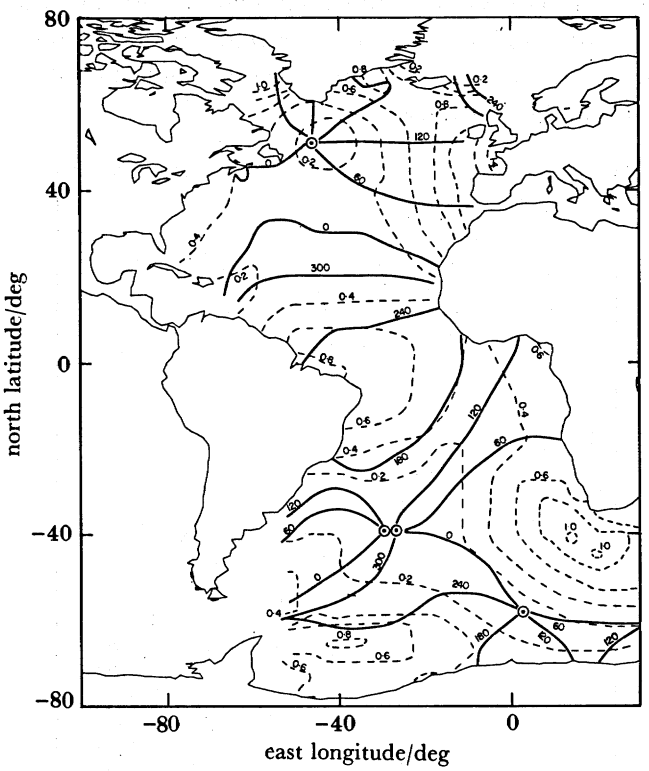

FIGURE 16. Tidal chart of the Atlantic Ocean for M_2 parametrized in terms of 20 Platzman normal modes. Solid lines show phase lags in degrees and dotted lines show amplitudes in metres.

The corresponding fit to Atlantic M_2 data is shown in figure 16 which uses modes 22–41 of Platzman *et al.* (1981) (37–56 of Platzman (1985)), in the range 17.7–10.1 h. Although there is a general similarity to the spatial distribution of Schwiderski (1983) in the locations of the major amphidromic centres and high amplitude areas, there are several significant differences not well reconstructed in the present case. These include the phase lag in the area to the south of the major North Atlantic amphidrome where there are few measurements and for which the fitted phase is systematically larger than that of the model; the double amphidrome of the central South Atlantic compared to the clear meridional separation of the two amphidromes in the model, and the large amplitude area to the south of the Cape of Good Hope. This latter feature was also obtained in fits to Atlantic M_2 altimeter data in Woodworth & Cartwright (1986). The r.m.s. residual error of the fit is also poor (23 cm), and of a similar magnitude to that obtained using the same number of Proudman functions, thereby suggesting that there is little increased efficiency in the use of the normal modes. Most of this residual variance is associated with the high amplitude, rapidly changing phase areas around Greenland, the Amazon and the Gulf of Maine. Increasing the number of modes used in the fit to 40 (modes 12–51) reduces the r.m.s. residual error to 19 cm with a similar geographical distribution of remaining variance, improves the phase distribution of the North Atlantic and separates the double amphidrome of the central South Atlantic, but enlarges the high amplitudes of the

Cape of Good Hope region. Quantitatively and qualitatively, therefore, the normal mode fits to the Atlantic M_2 data are by no means as successful as the O_1 fits.

(*e*) *Work done by the Moon*

No treatise on the ocean tides is complete without some examination of the work done by the moon in driving the major tidal harmonics in the region considered, and hence its contribution to the energy budget of the Earth–Moon dynamical system with all its geophysical implications (see, for example, Brosche & Sundermann 1978, 1981). We cannot of course give a global integral which is the ultimate geophysical goal, but it is interesting to map the distribution of work done over our best spatial synthesis for M_2. We use the representation of Proudman functions because these have no *a priori* constraints to their dynamical implications. Absence of radiation across the boundaries of the open parts of Rao's grid should, on an empirical fit to data, be compensated by artificial internal friction which is easily accommodated by the basis functions.

The work done by the Moon (or Sun) per unit area can be expressed

$$W = \rho(\overline{V\partial\xi/\partial t}), \tag{19}$$

where the overbar denotes a time-average, ρ is the density of sea-water (taken as 1025 kg m^{-3}, ξ is the ocean tide and V is the tidal potential approximated by

$$V/g = 0.168\cos^2\theta\cos(\omega t+2\lambda)\text{ m for }M_2$$

and

$$V/g = 0.140\sin\theta\cos\theta\cos(\omega t+\lambda)\text{ m for }O_1, \tag{20}$$

where θ, λ are north latitude and east longitude respectively and ω is the angular velocity. Note that this neglects the effects of the loading tide deformation of the bottom which are locally small (Hendershott 1972).

Equation (19) reduces to

$$W = 0.1189\,H\cos^2\theta\sin(G+2\lambda)\text{ for }M_2$$

and

$$W = 0.0474\,H\sin\theta\cos\theta\sin(G+\lambda)\text{ for }O_1, \tag{21}$$

where if H, G denote respectively the amplitude of the constituent in metres and the phase lag with respect to Greenwich, then W will be determined in units of watts per square metre.

The geographical distributions of the work done by the Moon for M_2 and O_1 in the Atlantic Ocean are shown in figure 17*a*, *b* making use of the fitted amplitudes and phases for each constituent determined by the fitting to Proudman functions shown in figures 13 and 12*a* respectively. For comparison, figure 17*c*, *d* show the corresponding distributions calculated from the Schwiderski model. For M_2, the large positive inputs in the NE Atlantic and across the central and SE Atlantic, and the negative inputs in the NW and SW Atlantic, are major features which would probably be obtained from any parametrization of the Atlantic M_2 tide and which are, of course, reflections of uncontroversial large-scale features of the M_2 tidal charts. Consequently, while it may be difficult to make an overall estimate of work done in the Atlantic or the global Ocean by integration over the details of the tidal field, it is clearly possible to demonstrate which geographical areas are most important to that calculation.

The corresponding values for O_1 in the Atlantic are almost all less than 1 kilowatt per square kilometre in magnitude. (Work done at the O_1 frequency is normally regarded as trivial,

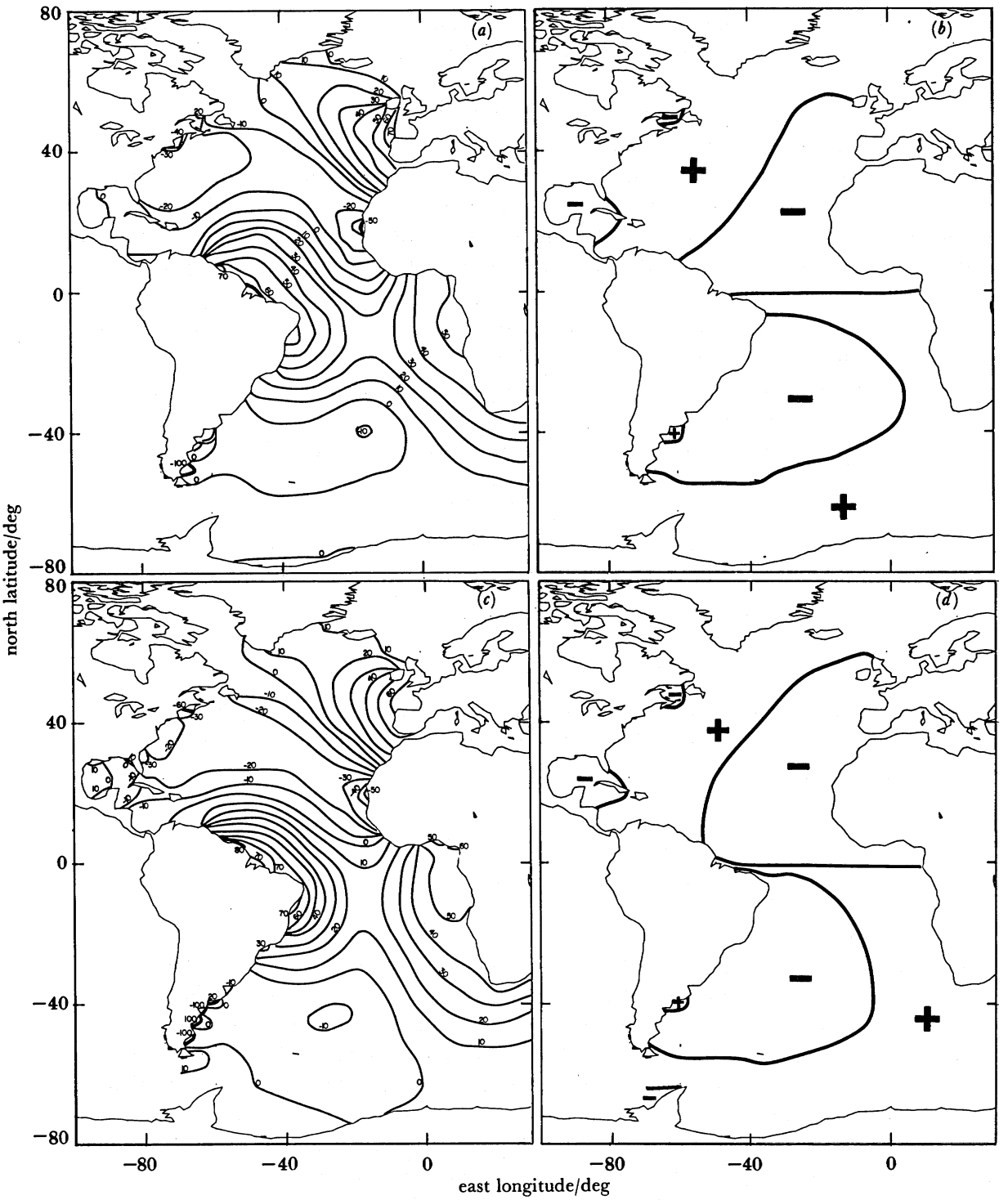

FIGURE 17. Work done by the Moon in kilowatts per square kilometre for (*a*) M_2 derived from figure 13; (*b*) O_1 derived from figure 12*a*; (*c*) M_2 taken from the Schwiderski model and (*d*) O_1 taken from the Schwiderski model.

PHILOSOPHICAL TRANSACTIONS OF THE ROYAL SOCIETY A MATHEMATICAL, PHYSICAL & ENGINEERING SCIENCES

but it is included here as an adjunct to our mapping of the O_1 constituent.) Figure 17*b*, *d* demonstrates simply the positive and negative input areas, in particular the positive inputs around Greenland, the western North Atlantic and the Southern Ocean together with the large negative input area in the western South Atlantic and the eastern North Atlantic. The distributions of work done for the other semidiurnal and diurnal constituents will be similar to those shown above to the extent that the M_2 and O_1 tidal charts are typical of all semidiurnal and diurnal tides.

6. Summary and conclusions

We have described and analysed an unprecedented large array of tidal pressure stations, concentrating in the main on their empirical strength, their relative precision, their complete span of the tidal spectrum, their subtle but interesting anomalies. This approach contrasts with the more usual one of dynamic modelling, where complete spatial coverage of a single harmonic is achieved at the expense of numerical and physical imperfections. However, we have gone some way towards a union of the two approaches by applying an objective analysis of all available data by fitting basis functions in the manner suggested by Sanchez *et al.* (1985), albeit with only part success. The fact remains that the ocean tides are known with great detail and precision at a finite number of points and only approximately elsewhere. At least, the density of measured points and the degree of approximation is obviously far better now in the Atlantic than in any other ocean.

When our programme first started seriously in 1968–1970 with pelagic measurements on the St Kilda shelf as described in C.E.S.V., there existed in the Atlantic Ocean only a few pioneering fragmentary pressure recorders by the French Navy on the north Biscay shelf and one or two by a United States NOAA team from George's Bank off Cape Cod, nothing in between. The few global computer models for M_2 differed radically from each other and from most data that were not used as rigid constraints. Having completed our programme, as far as official sanction and dwindling finances permit, the state of tidal knowledge is quite different. Notwithstanding some large areas of ocean still devoid of measurement, notably in the South Indian and South Pacific oceans, there now exist over 200 well-recorded pelagic stations worldwide (Cartwright & Zetler 1985), while great advances in modelling technique and physical realism have resulted in at least two very plausible models of the spatial pattern of eight or more harmonic constituents (Schwiderski 1980, 1981, 1982, 1983; Parke & Hendershott 1980; Parke 1982). One of the principal motivations for the new wave of tidal research in the 1960s and 1970s was to quantify the long-disputed energy dissipation, but by 1980 new techniques of satellite- and space-geodesy had been evolved to give what appear to be reliable, if still somewhat variable, estimates of the tidal torque on the Earth–Moon rotation (Lambeck 1977; Brosche & Sundermann 1978, 1981).

Of course, pelagic tidal data are still valuable in terms of their intrinsic physics and as constraints to various geophysical parameters which are affected by them. The most urgent requirement at the present time is to supply corrections to forthcoming exercises in satellite altimetry, where a precision of a few centimetres is necessary for more general oceanographic analysis. Although the frequency of the tides is much higher than other oceanographic signals in ocean topography they are strongly aliased by the periodicity of satellite orbits into very low frequencies which contaminate other signals of interest and are not easily removed by simple

PHILOSOPHICAL TRANSACTIONS OF THE ROYAL SOCIETY A MATHEMATICAL, PHYSICAL & ENGINEERING SCIENCES

averaging (Parke & Rao 1983). Parke & Hendershott (1980) demonstrate that their model for M_2 is imprecise to an order of 0.1 m amplitude or 10° in phase at mid-ocean islands, while comparison of Schwiderski's (1980) model with recent pelagic data shows that it produces errors of similar magnitude (Woodworth 1985). Parke (personal communication) has shown that the two models for M_2 differ vectorially by up to 0.4 m in certain large areas. The best models available, therefore, are not accurate enough to supply really satisfactory corrections to modern altimetry, although Parke & Hendershott (1980) do allow for the distinction between the geocentric tide sensed by altimetry and the tide relative to the sea bed provided by direct measurements. Thus, further pelagic measurements are justified, at least in the more neglected ocean areas, and improved computer models are needed to make the best possible use of the pelagic data already available. In this respect, the use of inverse methods in tidal analysis (Bennett & McIntosh 1982) has not yet been explored on an oceanic scale.

Another relevant aspect of satellite altimetry is that it promises to provide sufficient data within the next decade to make an independent assessment of the tidal field, perhaps globally, from analysis of the altimetry itself (Mazzega 1985; Woodworth & Cartwright 1986). If precise enough, this would provide a different role for the oceanographic tidal data, namely to quantify the tidal movement of the sea bed by subtracting the geocentric tide. At present, the earth tide is known only from inland tidal gravimetry. Tidal science, having sprung historically from astronomy, then having become a branch of geophysics and more particularly oceanography, is about to enter a new phase, as a part of space geodesy. Our laboriously acquired dataset should be relevant to all phases.

We are grateful to the many national authorities who have provided data from their tide-gauge networks and in some cases facilities on board their research ships for deploying our own instruments. Jean-Marc Verstraete of the 'Office de Recherche Scientifique et Technique Outre-Mer' let us use his data from tropical island sites. Alberto Franco, Afranio de Mesquita and Joseph Harari of the University of São Paulo helped in obtaining and analysing new data from the Brazilian shelf. We are specially indebted to Professor George Platzman of the University of Chicago and Dr D. B. Rao of the U.S. National Bureau of Meteorology for letting us use numerical data defining their oceanic basis functions. Our colleagues Peter Foden and Bev Hughes helped with instrument deployments at sea and calibration in the laboratory, and Claire MacDonald carried out most of the routine data processing.

The programme as a whole was supported financially by the U.K. Natural Environment Research Council through its 'science vote' budget.

Appendix A. Leading tidal constants from some islands and coastal sites

The tidal constants listed here are considered to be of superior quality to those from the same sites available from other sources if at all, either because of the long duration of their data or their instrumental quality. All analyses were performed by the authors, except for sites numbers 3 and 4 whose constants were provided by the Portuguese authorities. Sites 6, 10 and 11 are from offshore pressure records organized by J.-M. Verstraete of ORSTOM; in particular, number 6 (Natal) differs from other recordings there in being from the open sea outside the port area. Sites 13 and 14 are from recent long-term sea level recorders installed by IOS. The data from other sites were obtained by courtesy of the appropriate national authorities.

Table A 1 lists the geographical locations of the numbered sites, the number of years of data analysed and their approximate dates. Table A 2 lists amplitude in millimetres (upper figures) and Greenwich phase lag G in degrees (lower figures) for four leading diurnal, four leading semidiurnal constituents and M_3.

TABLE A 1. SPECIFICATION OF RECORDING SITES

1. St John's Harbour	47° 34′ N,	52° 41′ W	12 years	1962–1973
2. Bermuda (St George)	32° 22′ N,	62° 42′ W	10 years	1950–1959
3. Flores Island	39° 28′ N,	31° 07′ W	1 year	1977
4. Madeira (Funchal)	32° 38′ N,	16° 55′ W	1 year	1977
5. Sidi Ifni (Spanish West Africa)	29° 22′ N,	10° 12′ W	0.75 years	1963
6. Natal, Brazil	05° 46′ S,	35° 11′ W	1 year	1983–1984
7. Fernando de Noronha	03° 50′ S	32° 24′ W	1 year	1974
8. Ilha da Trindade	20° 30′ S,	29° 20′ W	1 year	1972
9. Ascension Island	07° 55′ S,	14° 25′ W	1 year	1983–1984
10. São Tomé (south point)	00° 02′ N,	06° 32′ E	1 year	1983–1984
11. Annobon Island[a]	01° 25′ S,	05° 37′ E	1 year	1983–1984
12. Pointe Noire, Congo	04° 48′ S,	11° 50′ E	1 year	1978–1979
13. Saint Helena (Jamestown)	15° 55′ S,	05° 42′ W	1 year	1986–1987
14. Tristan da Cunha	37° 03′ S,	12° 18′ W	1 year	1984–1985
15. Cananeia, Brazil	25° 01′ S,	47° 55′ W	9 years	1955–1963
16. Port Nolloth, RSA	29° 15′ S,	16° 52′ E	9 years	1968–1976

[a] This is sometimes called Pagalu.

TABLE A 2. AMPLITUDES (H) AND PHASES (G)

serial	Q_1	O_1	P_1	K_1	N_2	M_2	S_2	K_2	M_3
1	10	68	26	77	71	353	145	42	11
	89	129	157	161	302	316	360	359	243
2	12	54	21	66	82	357	81	22	1
	183	192	188	187	338	358	24	23	75
3	7	14	10	33	83	382	137	38	3
	261	336	93	99	45	59	78	75	145
4	15	46	19	61	153	721	268	73	3
	247	305	39	47	31	46	67	65	122
5	19	57	20	62	197	935	349	95	4
	254	294	40	43	28	43	67	65	199
6	11	51	15	49	167	805	266	78	6
	165	197	267	276	195	207	229	224	263
7	13	49	18	54	169	809	258	73	5
	167	202	278	282	192	206	227	222	266
8	15	55	10	30	68	398	154	42	4
	114	148	216	224	187	188	202	200	220
9	7	27	15	51	74	331	118	35	1
	136	194	315	326	165	178	201	194	89
10	3	18	34	114	108	504	164	49	2
	272	150	230	236	148	175	246	241	102
11	4	14	30	107	105	483	155	43	2
	345	183	224	228	209	208	229	219	146
12	5	14	29	99	102	523	168	52	2
	153	288	353	360	78	84	113	108	202
13	10	21	9	34	67	320	101	31	2
	143	188	340	349	70	80	99	94	75
14	4	17	5	20	54	221	85	26	5
	76	100	116	140	357	15	33	30	93
15	28	113	23	64	60	362	230	77	69
	104	126	187	191	247	181	184	196	8
16	10	19	13	54	120	546	231	64	7
	206	223	92	92	22	33	51	47	290

PHILOSOPHICAL TRANSACTIONS OF THE ROYAL SOCIETY A MATHEMATICAL, PHYSICAL & ENGINEERING SCIENCES

TABLE B 1

serial	code	latitude	longitude	depth	M_3	M_4
1.1.84	SG4	63° 08′	0° 00′	1579	3, 141	3, 135
83[a]	SG1	61 30	0 −01	190	4, 161	1, 207
82	SF3	61 24	2 06	1025	5, 143	1, 050
80	SE3	60 32	4 59	1027	7, 133	3, 321
78	SC4	59 12	7 41	1095	8, 107	4, 046
77[a]	SC1	58 59	7 24	206	10, 103	3, 075
76	SB5	58 12	9 58	1870	11, 102	4, 017
71	YN	57 09	10 06	2120	8, 084	8, 037
63	L	55 40	10 49	2504	8, 066	9, 034
60[a]	KM	51 08	9 48	117	10, 012	28, 264
59[a]	KL	48 48	7 01	125	11, 003	23, 196
52	IPD	47 51	10 23	3830	8, 338	8, 305
69	Y1	44 56	15 35	3160	5, 327	4, 254
74	IBW	40 18	15 03	5475	2, 293	6, 171
67	AS	43 02	21 52	2480	2, 258	2, 171
72	Y2	33 59	29 24	3294	5, 143	3, 080
70	A6	34 00	34 53	3066	5, 142	3, 048
28	R2	62 57	10 57	444	6, 102	8, 034
29	R1	62 50	24 43	493	5, 214	5, 163
30	D9	60 12	28 46	1200	3, 256	3, 170
31	D8	57 01	29 58	2448	2, 288	1, 204
32	D7	53 39	30 10	3196	1, 296	1, 150
37	RK	58 16	13 51	381	6, 079	7, 042
65	A3	43 06	35 11	3460	2, 164	3, 124
1.2.36	B2	44 29	40 30	2388	2, 165	4, 131
37	A1	46 04	46 34	515	2, 175	4, 144
33[a]	C	53 36	53 48	182	3, 219	3, 292
34[a]	GB1	47 00	51 35	135	12, 240	11, 195
22[a]	BB1	44 35	57 41	64	1, 216	1, 230
26[a]	GEOB	40 44	66 50	180	1, 103	3, 235
47	HEJK	62 10	62 58	349	3, 072	8, 041
10	EDIE	26 28	69 20	5421	1, 048	1, 262
7	REKO	27 58	69 40	5461	2, 038	1, 278
5	AML3	28 14	67 32	5242	1, 069	1, 354
4	AML1	28 08	69 45	5453	2, 036	1, 330
38	A7	33 55	41 12	3372	4, 139	2, 053
39	G1	26 35	43 58	3600	3, 141	3, 360
1.3.12	G2	19 00	47 31	3470	1, 304	1, 010
13	G3	14 42	48 50	3527	3, 315	3, 119
14	G4	9 59	50 31	4850	5, 305	3, 148
15	G5	7 00	51 33	3764	8, 310	3, 111
5	T1	10 05	17 14	527	2, 048	7, 214
6	T2	6 04	20 58	3650	1, 038	5, 181
7	T3	3 08	25 04	4200	2, 298	4, 162
8	T4	0 56	29 17	351	4, 284	3, 145
9	T6	−6 −45	34 18	2825	5, 250	6, 330
10	T7	−17 −04	13 40	2800	2, 097	2, 033
11	HB	−18 −03	36 08	152	6, 227	7, 323
16	FP1	0 01	20 01	2750	0, 339	7, 127
17	FP3	−0 −01	9 59	4100	3, 061	7, 132
18	FP4	0 01	−6 −00	3065	2, 153	13, 318
1.4.03[a]	PARA	−26 −18	47 31	74	39, 300	40, 293
4[a]	FLOR	−28 −38	47 31	190	8, 289	20, 154

[a] Continental shelf stations.

PHILOSOPHICAL TRANSACTIONS OF THE ROYAL SOCIETY A MATHEMATICAL, PHYSICAL & ENGINEERING SCIENCES

Appendix B. M_3 and M_4 at pelagic stations

Table B 1 lists the amplitudes and phases of the higher-order constituents M_3 and M_4 from most of the deeper pelagic pressure stations taken by IOS. Four stations from the outer British shelf, four from the Canadian shelf, two from the Brazilian shelf, and four MODE stations from table 3 of Zetler *et al.* (1975) have been added to supplement the geographical coverage. The three-tier serial numbers are those used in IAPSO *Publications Scientifiques* nos 30 and 33, where the principal tidal constituents are listed. Code letters and numbers are station numbers used internally by the originating institutions. South latitude and east longitude are given minus signs. Depths are given in metres, in some cases only approximately. Amplitudes H are given in units of 0.1 millibar (or approximately 1 millimetre) units and Greenwich phase lags G are given in degrees, in that order.

References

Accad, Y. & Pekeris, C. L. 1978 Solution of the tidal equations for the M_2 and S_2 tides in the world oceans. *Phil. Trans. R. Soc. Lond.* A**290**, 235–266.

Agnew, D. C. & Farrell, W. E. 1978 Self-consistent equilibrium ocean tides. *Geophys. Jl R. astr. Soc.* **55**, 171–181.

ATT 1986 *Admiralty tide tables*. Published by the Hydrographer of the British Navy (3 volumes).

Bennett, A. F. & McIntosh, P. C. 1982 Open ocean modelling as an inverse problem: tidal theory. *J. phys. Oceanogr.* **12** (10), 1004–1018.

Brosche, P. & Sundermann, J. (eds) 1978 *Tidal friction and the Earth's rotation*. I. (243 pages.) Berlin: Springer-Verlag.

Brosche, P. & Sundermann, J. (eds) 1981 *Tidal friction and the Earth's rotation*. II. (345 pages.) Berlin: Springer-Verlag.

Cartwright, D. E. 1968 A unified analysis of tides and surges round north and east Britain. *Phil. Trans. R. Soc. Lond.* A**263**, 1–55.

Cartwright, D. E. 1971 Tides and waves in the vicinity of Saint Helena. *Phil. Trans. R. Soc. Lond.* A**270**, 603–649.

Cartwright, D. E. 1975 A subharmonic lunar tide in the seas off western Europe. *Nature, Lond.* **257** (5524), 277–280.

Cartwright, D. E. 1976 Anomalous M_1 tide at Lagos. *Nature, Lond.* **263** (5574), 217–218.

Cartwright, D. E. 1983 On the smoothing of climatological time series, with application to sea-level at Newlyn. *Geophys. Jl R. astr. Soc.* **75**, 639–658.

Cartwright, D. E. & Amin, M. 1986 *The variance of tidal harmonics*. *Dt. Hydrogr. Z.* **39** (6), 235–253.

Cartwright, D. E. & Edden, A. C. 1977 Spectroscopy of the tide generating potentials and their relationship to observed features. *Ann. Geophys.* **33** (1/2), 179–182.

Cartwright, D. E., Edden, A. C., Spencer, R. & Vassie, J. M. 1980 The tides of the northeast Atlantic Ocean. *Phil. Trans. R. Soc. Lond.* A**298**, 87–139.

Cartwright, D. E., Munk, W. H. & Zetler, B. D. 1969 Pelagic tidal measurements. *EOS, Wash. Trans. Am. geophys. Un.* **50** (7), 472–477.

Cartwright, D. E., Spencer, R. & Vassie, J. M. 1987 Pressure variations on the Atlantic Equator. *J. geophys. Res. – Oceans.* **92** (C1), 725–741.

Cartwright, D. E. & Tayler, R. J. 1971 New computations of the tide-generating potential. *Geophys. Jl R. astr. Soc.* **23** (1), 45–73.

Cartwright, D. E., Zetler, B. D. & Hamon, B. V. 1979 Pelagic tidal constants. *Int. Assoc. Phys. Sci. of the Oceans.* Pub. Sci. no. 30. (65 pages.)

Cartwright, D. E. & Zetler, B. D. 1985 Pelagic tidal constants. 2. *Int. Assoc. Phys. Sci. of the Oceans.* Pub. Sci. no. 33. (59 pages.)

Chapman, S. & Lindzen, R. S. 1970 *Atmospheric tides: thermal and gravitational*. (200 pages). Dordrecht: Reidel.

Davies, A. M., Sauvel, J. & Evans, J. 1985 Computing near coastal tidal dynamics from observations and a numerical model. *Continental Shelf Res.* **4** (3), 341–366.

Filloux, J. H. 1980 Pressure fluctuations on the open ocean floor over a broad frequency range: new program and early results. *J. phys. Oceanogr.* **10** (12), 1959–1971.

Garrett, C. J. R. 1972 Tidal resonance in the Bay of Fundy and Gulf of Maine. *Nature, Lond.* **238** (5365), 441–443.

Garrett, C. J. R. & Munk, W. H. 1971 The age of the tide and the 'Q' of the oceans. *Deep Sea Res.* **18**, 493–503.

Gill, A. E. 1979 A simple model for showing the effects of geometry on the ocean tides. *Proc. R. Soc. Lond.* A**367**, 549–571.

PHILOSOPHICAL TRANSACTIONS OF THE ROYAL SOCIETY A MATHEMATICAL, PHYSICAL & ENGINEERING SCIENCES

Hendershott, M. C. 1972 The effects of solid earth deformation on global ocean tides. *Geophys. Jl R. astr. Soc.* **29**, 389–402.

Huthnance, J. M. 1980 On shelf-sea 'resonance' with application to Brazilian M_3 tides. *Deep Sea Res.* **27**A, 347–366.

Huthnance, J. M. 1983 Simple models for Atlantic diurnal tides. *Deep Sea Res.* **30** (1), 15–29.

International Hydrographic Bureau 1979 Tidal constituent bank, station catalogue. Department Fisheries and Oceans, Ottawa, Canada (with later updates).

Lambeck, K. 1977 Tidal dissipation in the oceans: astronomical geophysical and oceanographic consequences. *Phil. Trans. R. Soc. Lond.* A**287**, 545–594.

Luther, D. S. 1980 *Observations of long period waves in the tropical oceans and atmosphere.* Woods Hole Oceanogr. Inst., Tech. rep. WHOI-80-17. (210 pages.)

Luther, D. S. & Wunsch, C. 1975 Tidal charts of the central Pacific Ocean. *J. phys. Oceanogr.* **5** (2), 222–230.

Lutjeharms, J. R. E., Stavropoulos, C. C. & Koltermann, K. P. 1985 Tidal measurements along the Antarctic coastline. In *Oceanology of the Antarctic shelf* (ed. S. S. Jacobs) (Antarctic Res. Ser. **43**), pp. 273–289. American Geophysics Union.

McCammon, C. & Wunsch, C. 1977 Tidal charts of the Indian Ocean north of 15° S. *J. geophys. Res.* **82** (37), 5993–5998.

McMurtree, R. & Webb, D. J. 1975 Tidal response functions around Australia from harmonic constants. *Aust. J. Marc. Freshwat. Res.* **26** (2), 245–269.

Mazzega, P. 1985 M_2 model of the global ocean tide derived from SEASAT altimetry. *Mar. Geodesy* **9**, 335–363.

Munk, W. H. & Cartwright, D. E. 1966 Tidal spectroscopy and prediction. *Phil. Trans. R. Soc. Lond.* A**259**, 533–581.

Parke, M. E. 1982 O_1, P_1, N_2 models of the global tide on an elastic Earth plus surface potential and spherical harmonic decompositions for M_2, S_2, K_1. *Mar. Geod.* **6** (1), 35–81.

Parke, M. E. & Hendershott, M. C. 1980 M_2, S_2, K_1 models of the global ocean tide on an elastic Earth. *Mar. Geod.* **3**, 379–408.

Parke, M. E. & Rao, D. B. (eds) 1983 *Report of the NASA Workshop on tidal research.* NASA-JPL Pub. no. 83-71

Pekeris, C. L. & Accad, Y. 1969 Solution of Laplace's equations for the M_2 tide in the world oceans. *Phil. Trans. R. Soc. Lond.* A**265**, 413–416.

Platzman, G. W. 1983 World ocean tides synthesized from normal models. *Science, Wash.* **220**, 602–604.

Platzman, G. W. 1984 Normal modes of the world ocean. III. A procedure for tidal synthesis. IV. Synthesis of diurnal and semi-diurnal tides. *J. phys. Oceanogr.* **14** (10), 1521–1550.

Platzman, G. W. 1985 Normal modes of the world ocean: maps and tables. Univ. Chicago, Dept. Geophys. Sciences, unpublished report 97 pages.

Platzman, G. W., Curtis, G. A., Hansen, K. S. & Slater, R. D. 1981 Normal modes of the world ocean. II. Description of modes in the period range 8–80 h. *J. phys. Oceanogr.* **11**, 579–603.

Proctor, R. & Wolf, J. 1984 Cotidal charts of the northeast Atlantic Ocean from a 2-dimensional model. (Abstract.) In *Int. Ass. Phys. Sci. of the Ocean, 18th UGGI General Assembly, Programme and Abstracts, Hamburg*, pp. 110–111. Procès-Verbaux: Association Internationale des Sciences Physiques de l'Ocean.

Proudman, J. 1917 On the dynamical equations of the tides, Parts I, II, III. *Proc. Lond. math. Soc.* **18**, 1–68.

Proudman, J. 1944 The tides of the Atlantic Ocean. (George Darwin lecture.) *Mon. Not. R. astr. Soc.* **104**, 244–256.

Sanchez, B. V., Rao, D. B. & Wolfson, P. G. 1985 Objective analysis for tides in a closed basin. *Mar. Geod.* **9** (1), 71–91.

Sanchez, B. V., Rao, D. B. & Steenrod, S. D. 1986 Tidal estimation in the Atlantic and Indian Oceans. *Mar. Geod.* **10**, 309–350.

Schwiderski, E. W. 1980 Ocean tides. I. Global tidal equations. II. A hydrodynamical interpolation model. *Mar. Geod.* **3**, 161–255.

Schwiderski, E. W. 1981 *Global ocean tides: atlas of tidal charts and maps. Parts II–IX.* Naval Surface Weapons Centre, Dahlgren, Virginia. Rep. nos NSWC TR 81–122, 142, 144, 218, 220, 222, 224.

Schwiderski, E. W. 1982 *Global ocean tides: atlas of tidal charts and maps. Part X. The fortnightly lunar tide Mf.* Naval Surface Weapons Centre, Dahlgren, Virginia. Rep. no. NSWC TR 82–151.

Schwiderski, E. W. 1983 Atlas of ocean tidal charts and maps. Part I. The semidiurnal principal lunar tide M_2. *Mar. Geod.* **6**, 3–4, 219–265.

Spencer, R. & Vassie, J. M. 1985 Comparison of sea-level measurements obtained from deep pressure sensors. In *Advances in underwater technology and offshore engineering*, vol. 4, pp. 183–207. London: Graham and Trotman.

Vassie, J. M. 1982 Tides and low frequency variations in the equatorial Atlantic. *Oceanologica Acta* **5** (1), 3–6.

Webb, D. J. 1973 On the age of the semi-diurnal tide. *Deep Sea Res.* **20** (9), 847–852.

Whewell, W. 1833 Essay towards a first approximation to a map of cotidal lines. *Phil. Trans. R. Soc.* **123**, 147–236.

Woodworth, P. L. 1985 Accuracy of existing ocean tide models. In *Proc. Conf. on the use of satellite data on climate models, Alpbach, Austria.* SP-244, pp. 95–98. European Space Agency.

Woodworth, P. L. & Cartwright, D. E. 1986 Extraction of the M_2 ocean tide from SEASAT altimeter data. *Geophys. Jl R. astr. Soc.* **84**, 227–255.

PHILOSOPHICAL TRANSACTIONS OF THE ROYAL SOCIETY A MATHEMATICAL, PHYSICAL & ENGINEERING SCIENCES

Wunsch, C. 1967 The long-period tides. *Rev. Geophys.* **5** (4), 447–475.
Zahel, W. 1978 The influences of solid earth deformations on semi-diurnal and diurnal oceanic tides. In *Tidal friction and the Earth's rotation*, pp. 98–124. Berlin: Springer-Verlag.
Zetler, B. D. 1971 Radiational ocean tides along the coasts of the United States. *J. phys. Oceanogr.* **1** (1), 34–38.
Zetler, B. D., Munk, W., Mofjeld, H., Brown, W. & Dormer, F. 1975 MODE tides. *J. phys. Oceanogr.* **5** (3), 430–441.

PHILOSOPHICAL TRANSACTIONS OF THE ROYAL SOCIETY A MATHEMATICAL, PHYSICAL & ENGINEERING SCIENCES